



Master Thesis

Simon Glanzer (0830726)
simon.glanzer@edu.uni-graz.at



Karl-Franzens-Universität Graz
Institut für Chemie
Heinrichstraße 28/ II
8010 Graz, Austria

Contents

1	NMR diffusion measurements of macrolide antibiotics in bile acid micelles	1
1.1	Introduction	1
1.2	Methods	4
1.3	Results and Discussion	6
1.3.1	Degradation of Macrolide Antibiotics by using Bile Acids	8
1.3.2	Concentration measurements	9
1.3.3	Diffusion measurements	12
1.3.4	CMC measurements	15
1.3.5	Diffusion coefficients of macrolides and bile salts	17
1.3.6	Mole fraction partition coefficient calculations	20
1.4	Conclusion	22
2	A general method for diagonal peak suppression in homonuclear correlated NMR spectra by spatially and frequency selective pulses	23
2.1	Introduction	23
2.2	Theory and method	24
2.3	Results and discussion	29
2.4	Conclusions	33

1 NMR diffusion measurements of macrolide antibiotics in bile acid micelles

1.1 Introduction

Macrolide antibiotics are a powerful tool in medicine to treat gram positive and gram, negative bacterial induced diseases. By inhibiting the bacterial ribosomes, they stop the protein production of the bacteria [1]. Unfortunately, the treatment is accompanied by several side-effects like phospholipidosis [2][3] and many gastrointestinal tract damages.

A previous paper reported a connection between bile acid efflux and hepatotoxicity, where drugs with inhibition-tendency of bile acid transport, show a higher risk of hepatotoxicity. Furthermore it's commonly known that at least 50% of the human total drug clearance is done via the biliary pathway. Nevertheless, there are still problems from connecting animals studies with predictions of the human toxicity [4]. The chemical structures of all macrolide antibiotics are very similar. They consist of a large lactone ring, with several hydroxy groups on C3, C5, C6, C11 and C12 and two sugar units, connected via the oxygen from the hydroxy group on C3 and C5. However, the missing sugar units of azithromycin aglycone and decladinosylazithromycin change the size and the polarity of the molecule drastically, leading to different behaviors during the experiments. The chemical structures of the macrolide antibiotics are shown in figure 1.

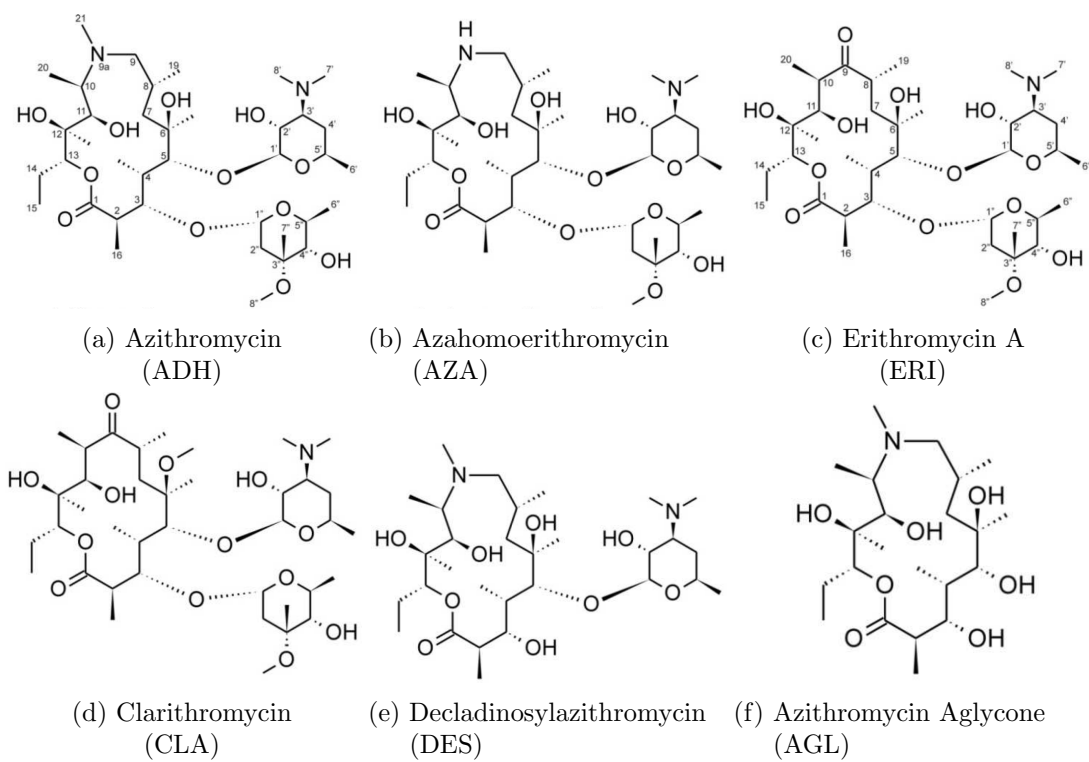


Figure 1: The investigated macrolide antibiotics in our experiments. Figures from [5].

Bile mainly consists of bile acids, where cholic acid and deoxycholic acid are the most abundant in mammals. The chemical structures of bile acids are derivatives of steroids. Figure 2 shows the structure of cholic- and deoxycholic acid. It consists of a hydrophobic nonaromatic four-ringssystem with hydrophilic hydroxygroups on one side and a side-chain with a carboxylic acid group. This amphiphilic character is the reason, why bile acids behave like detergents, by forming micelles with a hydrophobic core at certain concentrations (10-15mM NaCh, 4-7mM NaDCh). Because of this fact, the main physiological functions of bile acids are the solubilization and the transport of lipids in the body, by forming mixed micelles on one hand, but also the interaction with lipid soluble vitamins and drugs [6][7][8][9].

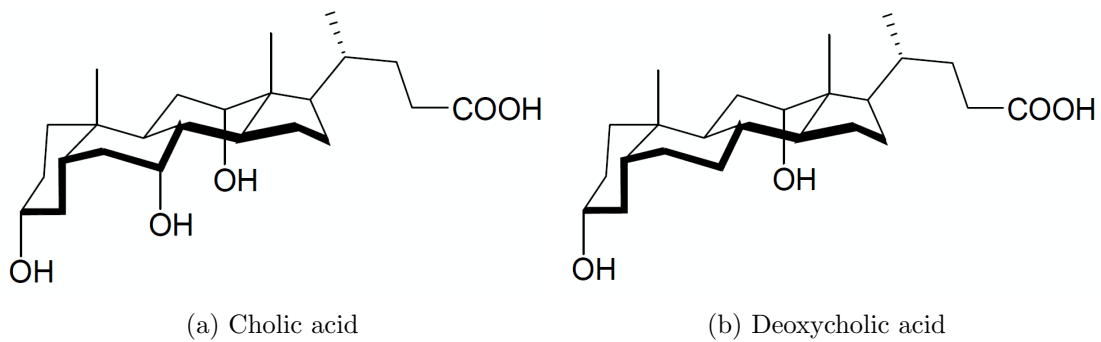


Figure 2: The two investigated bile acids in our experiments. Figures from [10].

Therefore, we hypothesized that the hydrophobic antibiotics can be bound analogously to the bile acids and can be delivered in these micelles during excretion[10].

1.2 Methods

The investigated macrolide antibiotics are azithromycin (in dihydrate form), decladinosylazithromycin, erythromycin A, azahomoerythromycin, clarithromycin and azithromycin aglycone (azithromycin from Fluka, *57947-1G*; all other macrolides were provided from the university). The bile acids in our experiments are cholic acid and deoxycholic acid. For the first measurements, we used the acids and mixed them with an adequate amount of 40 %wt. sodiumdehydroxid NaOD (NaOH would give rise to a huge water peak at 4,7 ppm). Overnight experiments showed that the macrolide antibiotics degrade during the experiment. A logical explanation for this degradation might be a base excess, caused by weighted portions near the uncertainty limit of the balance. The literature shows that at conditions over pH 8 macrolides starting to degrade [11]. Therefore, it is more convenient and safer to work with the corresponding bile salts directly, in our case sodiumcholate (NaCh) and sodiumdeoxycholate (NaDCh) (Sodium cholate hydrate from Sigma, *C1254-25G*, $\geq 99\%$ purity; deoxycholic acid sodium salt from Fluka, *30970*, $\geq 98\%$ purity)

Because of varying CMC values of cholate and deoxycholate in literature (cites in discussion section), we measured the CMC on our own by NMR diffusion measurements. Because the size of the bile acid micelles (and therefore also the diffusion coefficient) are concentration dependent, we used always the same concentration for our macrolide investigations. Investigations [12] were made on this dependence and the literature shows relatively stable micelles in respect of their size at about 100mM. Although the concentrations in human are lower (10-50mM in gall bladder, 5mM in gall capillaries and 4mM in the gut.[13] Because of the more hydrophobic character of NaDCh compared to NaCh (one OH group missing), bigger micelles are formed at same concentrations. In the case of NaDCh a 50mM solution seemed sufficient enough.

For the experiments with macrolide antibiotics in the bile salt we dissolved the bile salt in D₂O (99.9%) at first. Because of the very poor solubility of the macrolides we added more than the solubility limit to the aqueous bile salt solution. After 15-30 minutes in the sonic bath, we centrifuged the remaining antibiotic to the bottom and pipetted the liquid part into the NMR tube. Previous experiments showed that it doesn't matter if we dissolve the antibiotic before or after the addition of bile salt. To eliminate the possibility of a degrading sample, we added a long 1D experiment after the DOSY experiment.

To measure the diffusion coefficient of the free macrolides, we have done the same procedure, but without adding bile salts.

For the concentration measurements of macrolides in the solution it was more convenient to set the bile salt as an internal standard with 100/50mM. By comparing the integrals of the bile salt signals with the macrolide peaks, we can quantify the soluble macrolide, presuming a linear correlation. Because of the different sizes of the molecules, varying delays during the experiments might lead to different results. Therefore different delay times were investigated.

All measurements were executed on a 500 MHz Bruker AVANCE III spectrometer. For the DOSY experiments we used a bipolar pulse pair longitudinal eddy current delay (BPP-LED) sequence. This sequence is commonly used for DOSY experiments. It features some improvements on resolution and a solution of problems with the eddy current on a normal DOSY experiment. A normal field gradient pulse is replaced by two gradients half the strength and a 180° pulse between them. In order to avoid the strong transverse relaxation during τ_2 , the magnetization is transferred into the z-direction by a 90° pulse before. More detailed descriptions are in NMR DOSY literature [14]. The concentration measurements are acquired without water suppression, because otherwise compound peaks near 4,7 ppm could get suppressed too, leading to false concentration measurements.

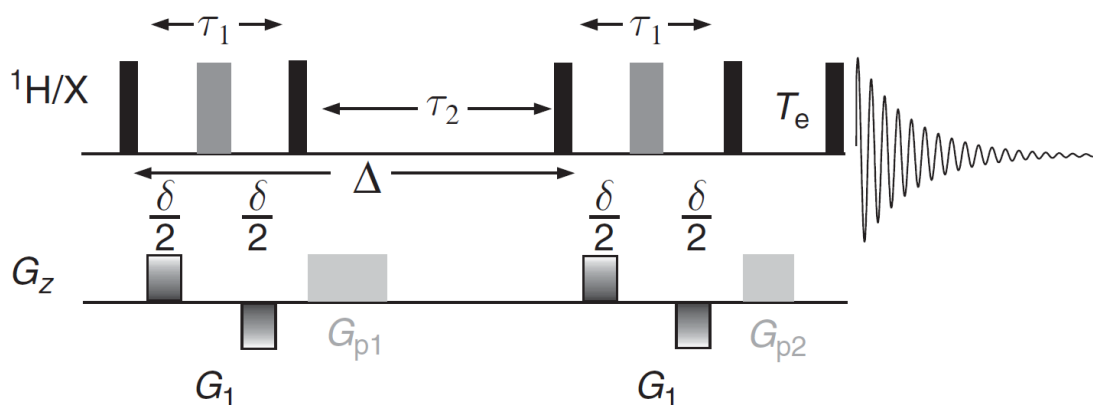


Figure 3: The BPP-LED pulse sequence used in our DOSY experiments.

1.3 Results and Discussion

Figure 4a shows a spectrum of sodiumcholate. The three OH units are well separated from the rest of the spectrum at 4.0, 3.8 and 3.4 ppm. Furthermore, the two methyl groups at 0.4 and 0.6 ppm are also good peaks to investigate. For the concentration studies, we need to divide the area of those methyl groups by a factor of three, to get the intensity of one single proton. All picked peaks are marked with a red arrow. In case of sodiumdeoxycholate of course, one OH signal at 3.8 ppm is missing and we took one peak at 2.2 ppm instead (orange arrow).

The spectra of macrolides (fig. 4b) are more complicated. Because all macrolides show different spectra, we took always different peaks for our interpretation. One very important role in our assignment plays the duplett at 5.0 ppm, which belongs to the hydrogen on C13 near the lactone group in case of AGL and DES. For the all other macrolides this hydrogen-duplett belongs to the carbon connecting one sugar unit (C1"). Although proximity to the water peak (and therefore influence by the water suppression) it is possible to monitor, if the ring conformation is stable during the whole experiment. Further calculations showed that the water suppression does also not influences the calculation of the diffusion coefficient of this peak.

Figure 4c shows a spectrum of erythromycine A in the presence of sodiumcholate. Because of the very poor solubility of the macrolides and the rather high concentration of bile acids (100mM), the bile acid peaks are huge in respect to the macrolide peaks. In many cases, its impossible to detect or reasonable measure the macrolide peak intensities. Fortunately, the spectrum of pure bile acid (fig. 4a) features a gap of peaks between 2.2 and 3.2 ppm and above 4.0 ppm. In this area observable macrolide peaks can be measured and selected with satisfying accuracy. It is possible to witness some very small peaks in this gap and also the duplett discussed above (blue arrows). However, unfortunately also in this bile acid peak free region impurities or satellite peaks can complicate measurements. Of course this imbalance of peak sizes decreases with better soluble macrolides like AGL or DES, but can cause great troubles in case of KLA and ADH experiments, where the solubility is very poor.

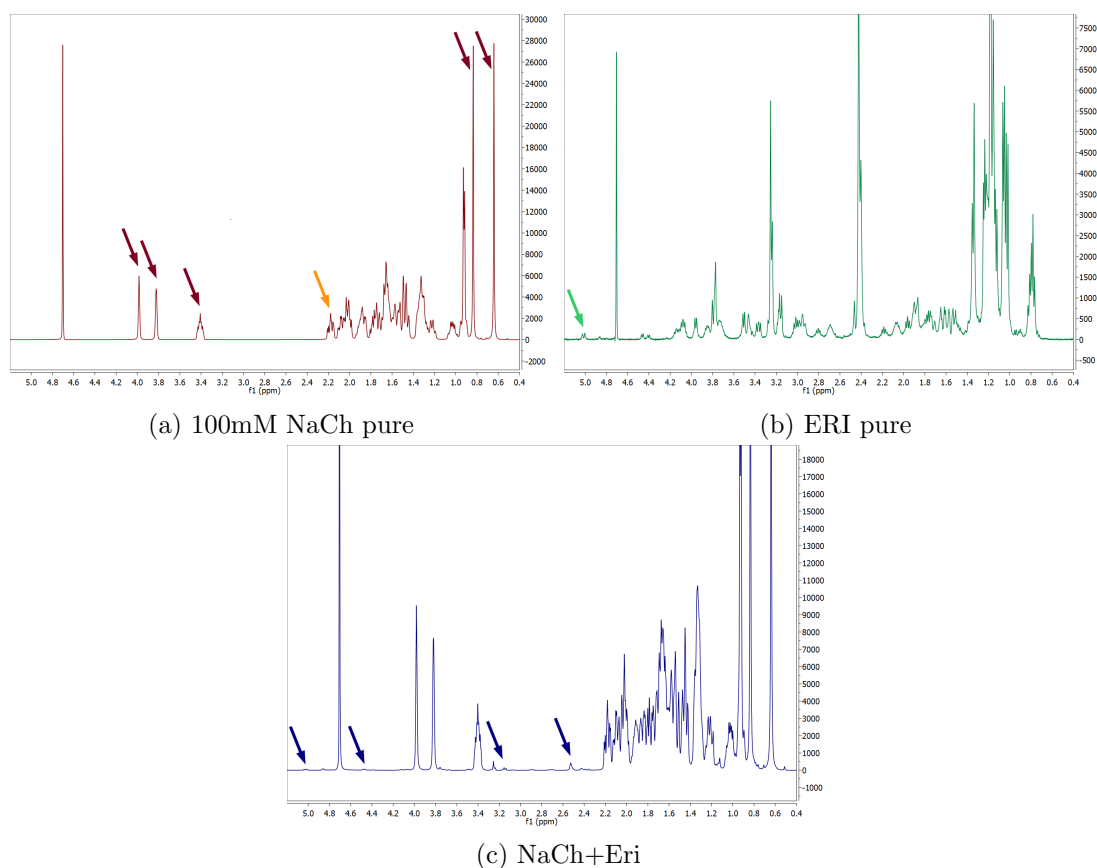


Figure 4: 1D spectra of erithromycin and sodiumcholate pure and in combination.

Figure 5 shows a stacked spectrum of all 1D spectra discussed above. Some macrolide peaks are easy to find in both spectra (blue and green), because they are separated enough from other peaks (5.0, 2.7 and 4.5 ppm). But for many peaks it is quite complicated to follow the peaks through both spectra. Because of the totally different chemical environment of micelles compared to pure water, the peaks can drift or change their shapes drastically.

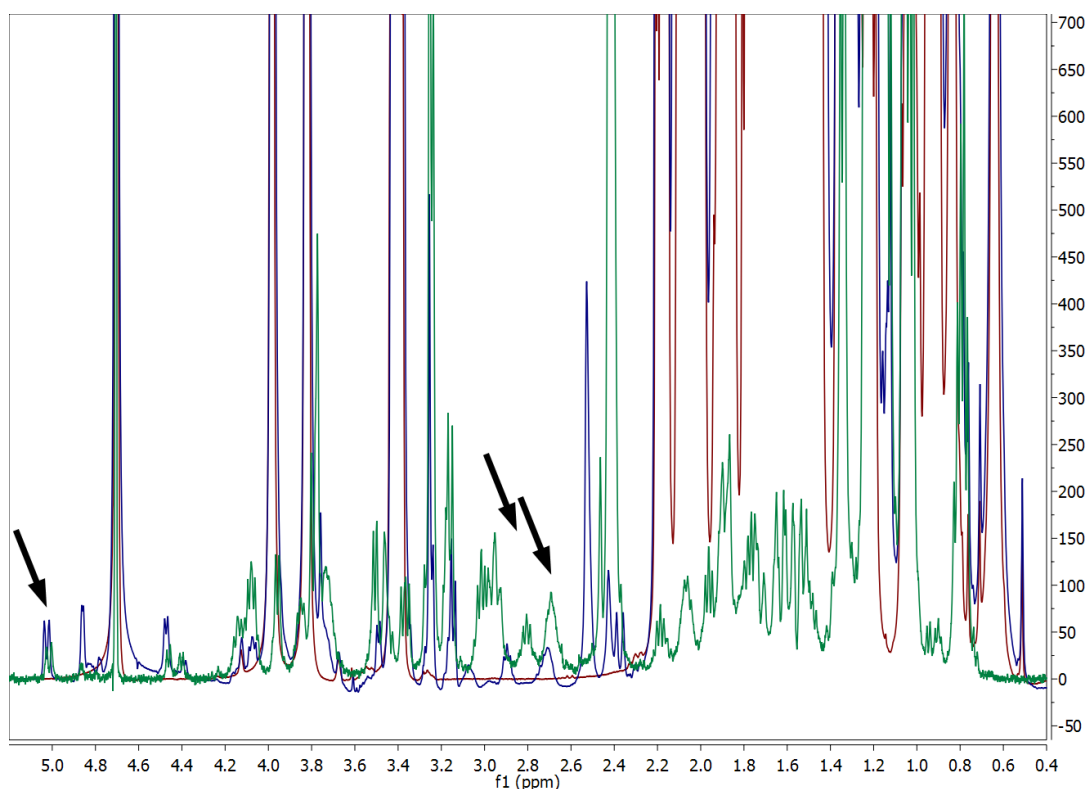


Figure 5: Stacked spectrum of the 1D spectra of figure 4. Red = NaCh, green = ERI, blue = NaCh+ ERI.

1.3.1 Degradation of Macrolide Antibiotics by using Bile Acids

As described in the method section, using the bile acid and deprotonating the acid with NaOD can cause high pH values. This alkaline conditions can ease the cleavage of the lactone unit, ending up with a ring opening hydrolysis. Figure 6 shows three different spectra from the same sample but with several hours in between (first red, then green, then blue). The marked peak at 5.0 ppm is the proton peak connected two the carbon near lactone unit. We can observe the vanishing of this peak after a period of time. Long DOSY experiments can not be done with this method!

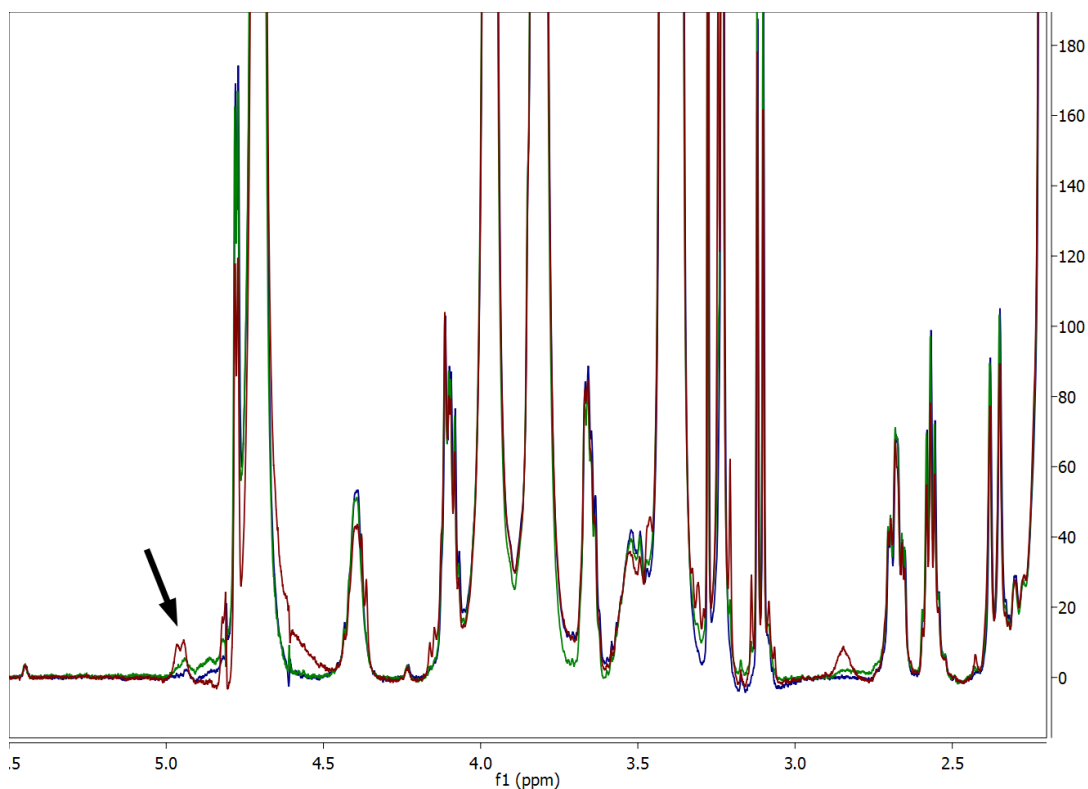


Figure 6: Spectra of the same sample (ERI+NaCh) in one our interval. First red, then green and then blue.

1.3.2 Concentration measurements

It's commonly known that the peak integrals in a compound mixture (with different molecule sizes) depend on the delay between the experiments. This is caused by the fact that bigger molecules undergo a faster relaxation, because of the higher spin density surrounding them. This faster decay of the spin signal yields after Fourier transformation a different area under the peak and we cannot compare the areas with a satisfying precision anymore. We acquired 1D spectra with varying delay times (1s, 7s, 20s, 40s) of random samples. The results of the concentration measurements are calculated as following:

$$c_{\text{macrolide}} = c_{\text{bile acid}} * \frac{\bar{A}_{\text{macrolide}}}{\bar{A}_{\text{bile acid}}} \quad (1)$$

$c_{\text{Bile acid}}$ is the concentration of cholate or deoxycholate in the sample (100mM and 50mM). For the mean values of the antibiotics $\bar{A}_{\text{Macrolide}}$ we measured the areas under

the highest and best separated peaks, which are changing from antibiotic to antibiotic. For values $\bar{A}_{\text{Bile acid}}$ we choose always the peaks at 0.7, 0.9, 3.8 and 4.0 ppm for NaCh and at 0.7, 0.9 and 3.8 ppm for NaDCh. The first two areas belong to methyl groups and must be divided by three. The calculation of standard deviation of $c_{\text{Macrolide}}$ is done by propagation of uncertainty with formula 2, where u is the uncertainty of the variables.

$$u_y = y \cdot \sqrt{\left(\frac{u_1}{x_1}\right)^2 + \left(\frac{u_2}{x_2}\right)^2} \quad y = x_1 : x_2 \quad (2)$$

Figure 7 shows the delay dependence of the concentration measurements of 4 random macrolide bile acid mixtures. Because the huge peaks of the bile salt are interfering with the areas of the small antibiotic peaks, the values of the standard deviation are very high (approx. 15%). The intensity of the uncertainties are changing from sample to sample, because some macrolides show bigger separated signals in the "bile acid gap" although the concentration is lower (e.g. NaDCh+KLA). We can see a quite good reproducibility when we look at the two different NaCh+ERI samples. But in all cases the delay effect is not visible or at least smaller than the inaccuracy of the experiment. Consequently 1D experiments with a delay of only one second are precise enough for our purposes.

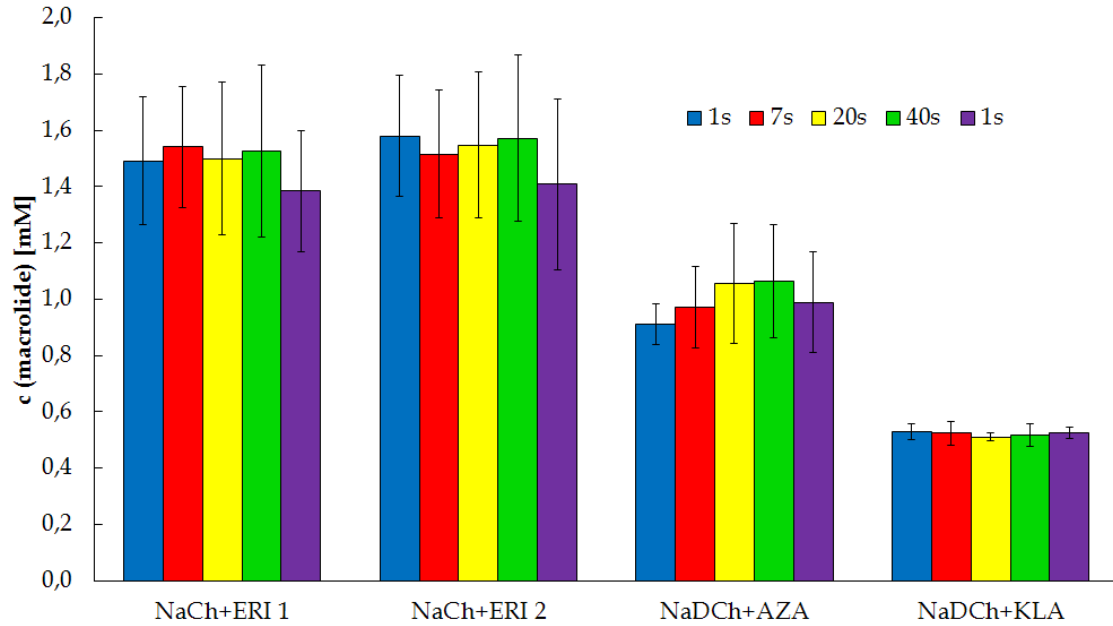


Figure 7: Delay-dependence on concentration measurements.

With this information we acquired 1D experiments of all 6 macrolides in both bile salts.

The mean values of the areas and their according concentrations (uncertainties included) are plotted in table 4 and 5 in the appendix. The data of both tables are shown in figure 8.

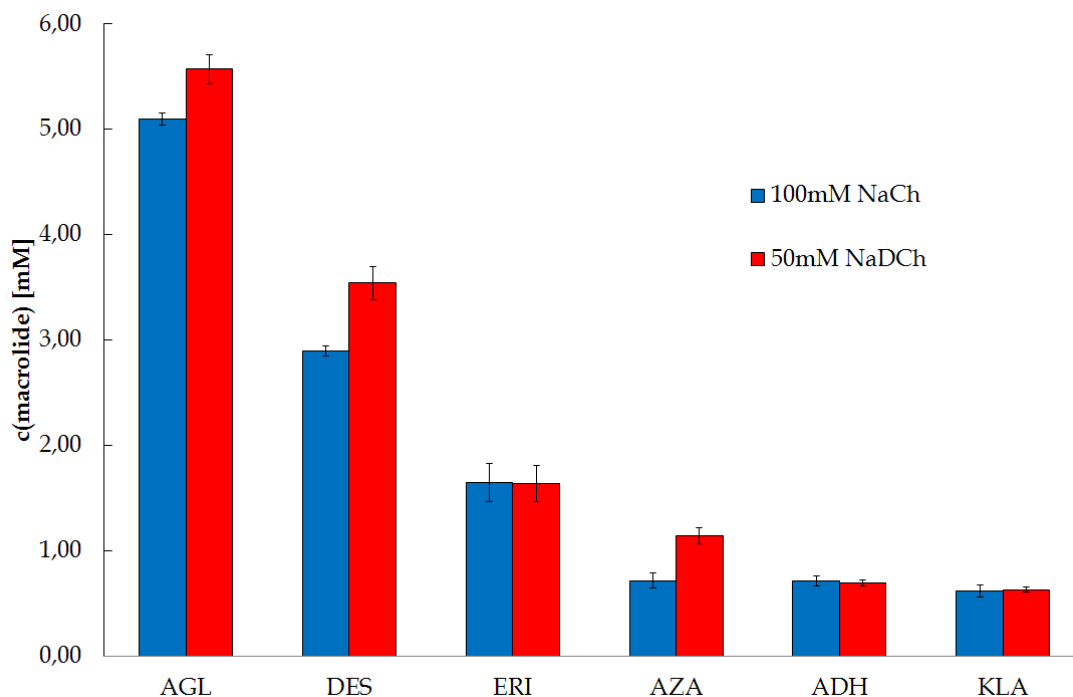


Figure 8: Concentrations of Macrolide antibiotic in presence of Bile Acid.

Aglycon shows the best solubility and clarithromycin the worst. It is also visible that all measurements underlies huge errors bars, caused by interfering bile acid peaks with the small macrolide peaks. Furthermore, the macrolide antibiotics show similar solubilities in both bile acids. It seems that the NaDCh increases the solubility a little bit, but the concentration difference is mainly on the edge of the error bars and therefore not reliable interpretable. All these phenomena can be explained by one physical effect: hydrophobicity. Starting our interpretation with erythromycin A, which yield average concentrations in our experiment. When we look at the chemical structure of ERI and replace the hydroxy group on C6 by a methoxy group, we result with clarithromycin, which is more apolar and therefore shows a poorer solubility. Azahomoerythromycin has slightly differences to the erythromycin concerning the C9 position (no carbonyl but one additional aminogroup), but shows all in all a similar hydrophobicity and also their solubility is in the same region. Starting from AZA and replacing the Hydrogen of

the aminogroup by a methyl group (lowering the hydrophility), we end up in a poorer solubility (ADH). For the results of DES and AGL we have to keep in mind that the sugar units on the macrolides are highly substituted (only one OH group). That means, missing sugar units are raising the hydrophilicity and therefore raising the solubility, which is compatible with our results in figure 8.

1.3.3 Diffusion measurements

According to the discussed DOSY experiment, the left signal intensity in the spectrum is defined as in equation 3 [14]. I_G is the signal intensity with a certain gradient strength, γ the gyromagnetic ratio (for ^1H : $2.675 \cdot 10^8 \text{ s}^{-1}\text{T}^{-1}$), δ the diffusion delay, Δ the diffusion time, D the diffusion coefficient and G_{tot} the field gradient strength.

$$I_G = I_{G=0} \cdot e^{-(\gamma \cdot \delta \cdot G_{\text{tot}})^2 D (\Delta - \frac{\delta}{3})} \quad (3)$$

Because of the fact that all variables except the gradient strength are kept constant, we can rewrite the formula to equation 4. The intensity of the signal is only dependent on the relative strength of the field gradient G [%] and after taking the natural logarithm equation 5 results. K is now the experiment internal constant (at certain parameter values).

$$\frac{I_G}{I_{G=0}} = e^{-K \cdot G^2 \cdot D} \quad \text{where} \quad K = \left(\gamma \cdot \delta \cdot \frac{G_{\text{tot}}}{100\%} \right)^2 \left(\Delta - \frac{\delta}{3} \right) \quad (4)$$

$$\ln \left(\frac{I_G}{I_{G=0}} \right) = -K \cdot G^2 \cdot D \quad (5)$$

If we vary the relative gradient strength G now, the signal intensities must change according to equation 5. Figure 9 shows the same compound with the same internal constant but with different gradient strengths. We can observe, nearly all peaks are decreasing at the same rate except the water peak at 4.7 ppm. Because of the high diffusion coefficient of the water proton, the signal is gone at the fifth step.

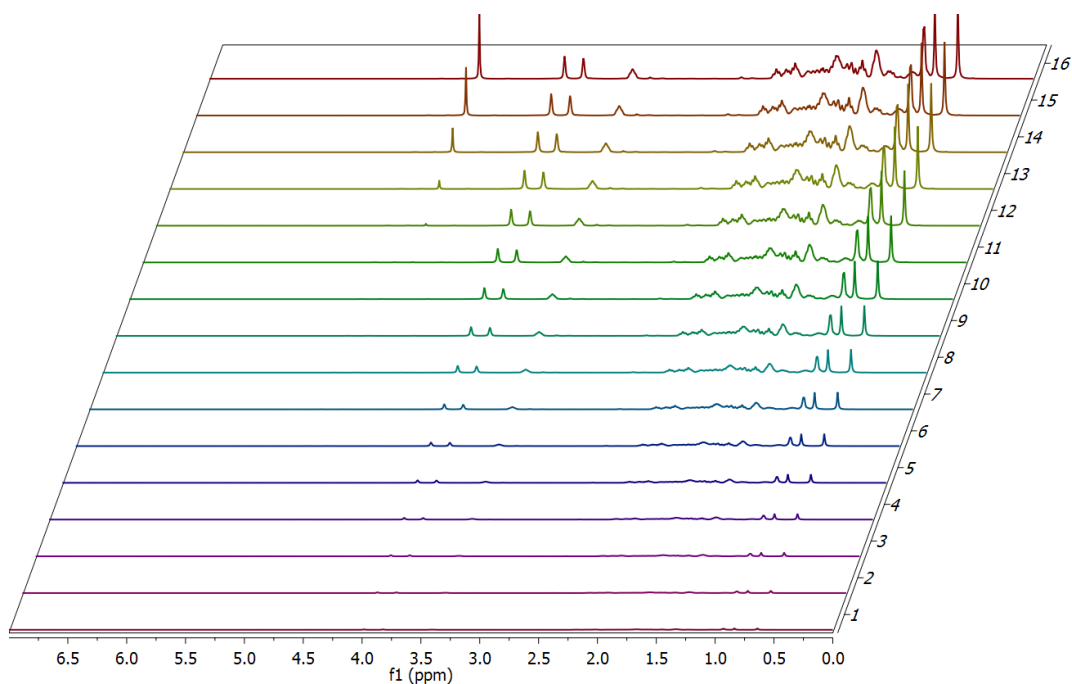


Figure 9: ERI+NaCh at gradient strengths varying from 2 to 95 %. G increases from top to bottom

We can follow this degradation at every peak in the spectrum, and can measure the degradation rate. To make these equations clearer, we plotted some results of a random DOSY experiment in to two different diagrams (figure 10) according to equation 4 and 5. The diffusion coefficient is temperature dependent. Because of this reason the temperature is kept constant at 298K (23°C) over all DOSY experiments.

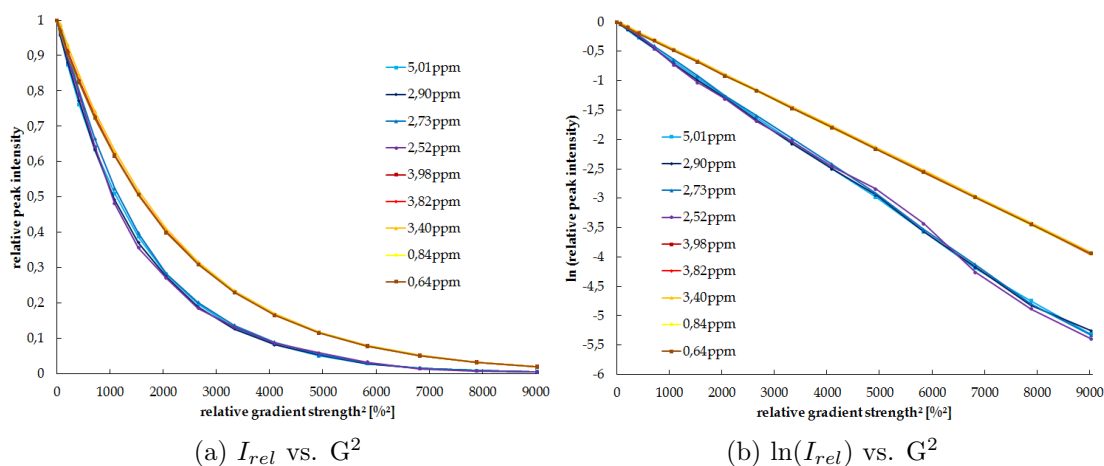


Figure 10: Decay measurements with increasing gradient strength of NaCh+AGL. It is clearly visible that the first 4 peaks have a different decay than the others and therefore belong to a molecule with a different diffusion coefficient.

The slope of diagram 10b according to equation 5 is $m = -K \cdot D$. With the known K value we can measure the slope and further calculate the diffusion coefficient of the molecules which belong to the measured signals. To get the best results, we had to calibrate our experiment first. Calibration means that with a gradient strength of 95% approximately 2 % of the relative signal intensity should remain. With the parameters $\delta = 0.004s$ and $\Delta = 0.1s$ this criteria is fulfilled and these parameters are kept constant over all DOSY experiments, leading always to the same internal constant K (in our case $2.58 \cdot 10^6 \text{ s/m}^2$).

It is possible to resolve the spectrum in respect of different diffusion coefficients on the computer directly and we get spectra like figure 11. In figure 11a (AGL+NaCh) it is possible to see compounds with 3 different diffusion coefficients. The peak width in the indirect dimension (y -axis) is rather high for all compounds, leading to huge uncertainties for the diffusion coefficients. The water peak in the left bottom corner is quite separated from the rest of the spectrum because of the high D (one order of magnitude). The other two compounds, are only well separated at regions, where no peaks from the other compound is interfering. In areas, where peaks from both compounds are abundant, the program has problems with processing the results. Keeping in mind that AGL is the best soluble macrolide and have a relative big difference in the diffusion coefficient compared with the bile acid, we can expect even more problems with macrolides with

poorer solubility and more similar diffusion coefficients. In figure 11b (ERI+NaCh) it is nearly impossible to detect the macrolide peaks or measure their diffusion coefficients. Because of this fact, the computer program for diffusion ordered 2D spectra is a nice tool for a quick overview of the matter. But for accurate results the processing must be done manually.

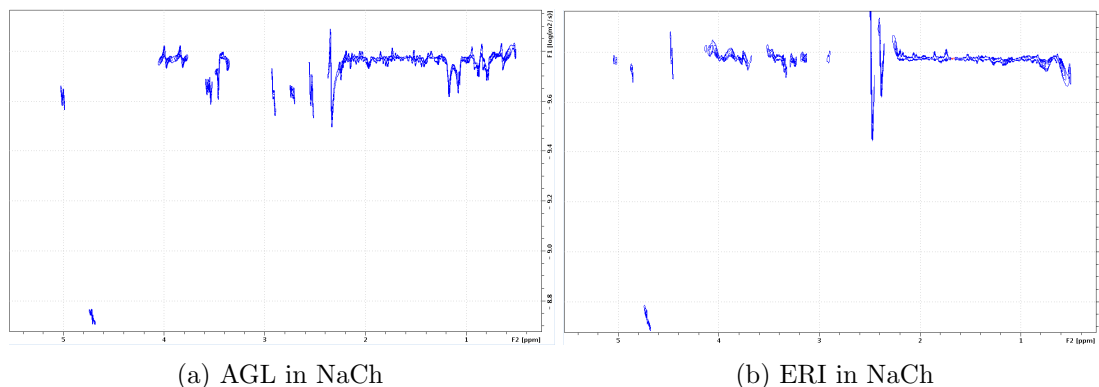


Figure 11: The results of the DOSY processing. The indirect dimension is the logarithm of the diffusion coefficient.

1.3.4 CMC measurements

For the CMC measurements (critical micelle concentration) we used the parameters discussed before. From previous works (table 1) we know that the CMC value of NaCh should be between 10-15 mM and of NaDCH around 5 mM. These values arose from conductometry, solubility measurements and other methods. Therefore we prepared bile salt samples near these concentrations. Under the CMC value, the molecules should have the same diffusion coefficient, independent on the concentration. But reaching the CMC, micelles starting to form, building bigger aggregations, and therefore lowering the average diffusion coefficient.

Table 6 and 7 in the appendix show the measured diffusion coefficients at certain concentrations. The diagrams in figure 12 visualize this dependence.

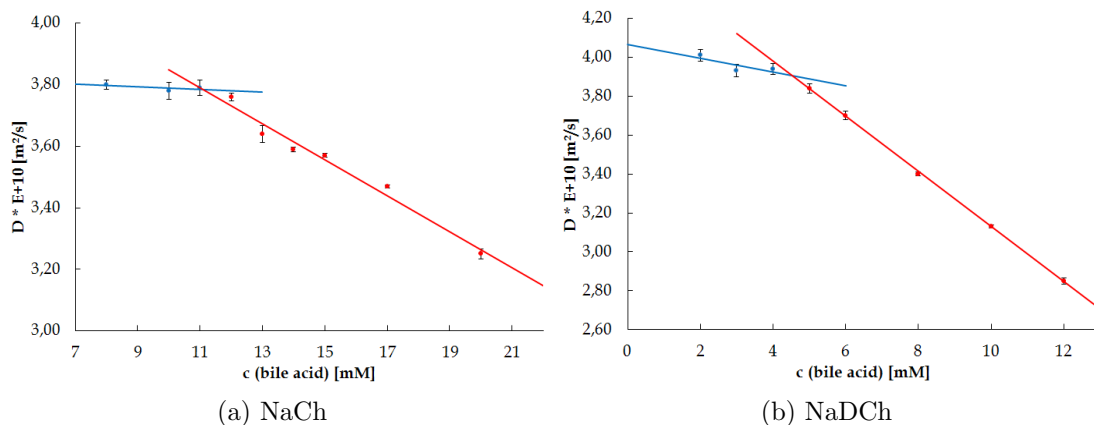


Figure 12: CMC measurements of bile acids.

The standard deviations (error bars) are not very high and therefore the diffusion coefficient for each concentration are quite reliable. The results for the NaCh suggest a CMC value of approximately 11mM and for NaDCh of about 4mM. These values are congruent with recent works (table 1), showing that our method for CMC determination is accurate but time consuming. The works were chosen randomly, but there are several more papers about the CMC determination of bile salts. But in many works the CMC of NaCh is approximately 10-19mM and of NaDCh approx. 4-5mM.

Table 1: Suggested CMC values (in mM) in literature.

CMC (NaCh)	CMC (NaDCh)	method	literature
14-15	4.5-5.5	potentiometric titration	[15]
14	4.1	fluorescence	[16]
19	4.8	Cholesterol Solubilization	[17]
19.7	13	freezing point depression	[18]
15	-	fluorescence	[19]
10	4.0	Isoth. Titr. Calorimetry	[20]
11	4.0	potentiometric titration	[21]
8.0	4.5	conductometry	[22]
13±1	3±1	diffusion measurements	[23]

1.3.5 Diffusion coefficients of macrolides and bile salts

We measured the diffusion coefficients of free macrolides, pure bile acid salts and macrolides mixed in bile salt micelles. The results for NaCh are visualized in figure 13. The exact values of the diffusion coefficients are gathered in table 8 in the appendix. Because not all bile salts are bound in the micelles, but also are free in solution, the diffusion coefficient resulting from the experiment can not be assumed as D of the micelles. The rate of the exchange from free to micelle bound bile salt is very fast (at least much faster than our experiment time) and therefore the diffusion coefficient of the bile acid D_{exp} is an average of both forms according to equation 6.

$$D_{\text{exp}} = D_{\text{free}} \cdot \frac{A_{\text{free}}}{A_{\text{tot}}} + D_{\text{bound}} \cdot \frac{A_{\text{bound}}}{A_{\text{tot}}} \quad , \quad A_{\text{tot}} = A_{\text{bound}} + A_{\text{free}} \quad (6)$$

D_{free} is the diffusion coefficient at the critical micelle concentration, A_{free} the concentration of free bile acid salt (which is the CMC, assuming that the amount of free bile acid is concentration independent). After setting A_{tot} as the total concentration of bile acid, A_{bound} to bile acid bound in the micelles and measuring D_{exp} , we can calculate D_{bound} , which is the real diffusion coefficient of the micelles. This D_{bound} must be the "minimum" of all our diffusion measurements. Table 2 shows the parameters and results for NaCh and NaDCh.

Table 2: Calculation of D of the micelles according to equation 6. All concentrations in [mM] and all diffusion coefficients in [m^2/s].

	A_{tot}	A_{free}	A_{bound}	D_{free}	D_{exp}	D_{bound}
NaCh	100	11	89	$3.79 \cdot 10^{-10}$	$1.70 \cdot 10^{-10}$	$1.44 \cdot 10^{-10}$
NaDCh	50	4	46	$3.96 \cdot 10^{-10}$	$1.43 \cdot 10^{-10}$	$1.21 \cdot 10^{-10}$

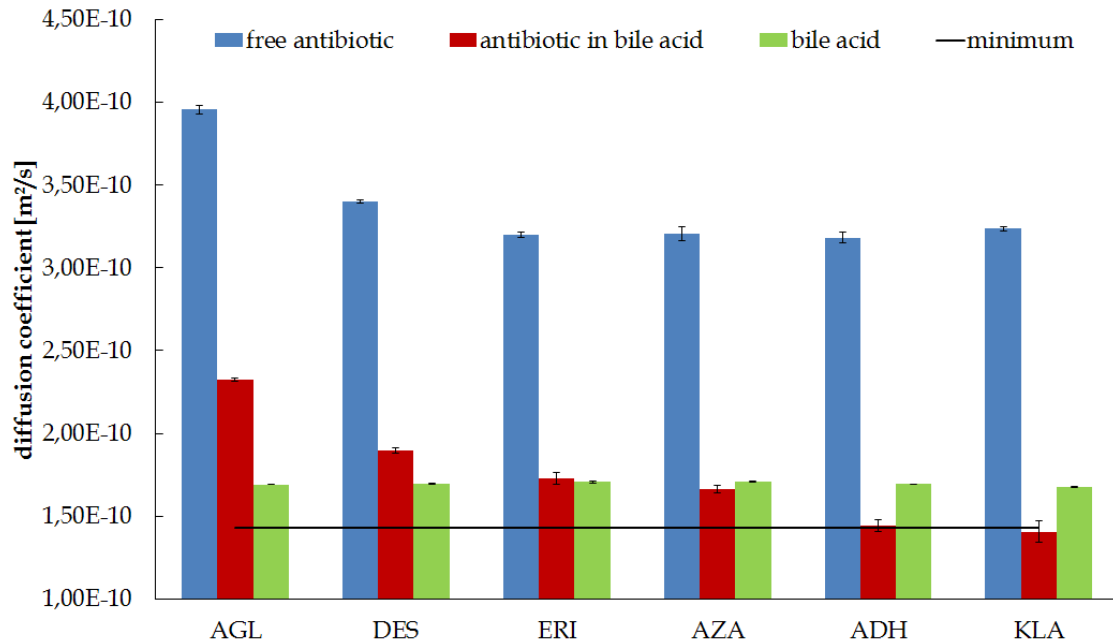


Figure 13: The overall results of all diffusion experiments with NaCh. The "minimum" is calculated with equation 6.

The results of the free antibiotics measurements are quite reasonable. It is well known that the size of the molecule is influencing the diffusion coefficient drastically. Because the macrolides are not really changing in respect to their size, it is also logical that they have similar diffusion coefficients. DES and AGL show higher diffusions, which can be explained by their missing sugar units and therefore smaller size. We can also observe in this diagram that the measurement of the diffusion coefficient of the bile salt (with high concentration) is not changing over all experiments. This means, different macrolides do not change the size of the micelles. The standard deviation is really small and in different experiments the diffusion coefficient of the bile salt is extremely stable. This fact indicates that our method is reliable and reproducible, if the concentrations are in acceptable regions.

When we look at the diffusion coefficients of antibiotics in combination with bile salt we see that D is in between D of free antibiotic and D of the micelles (minimum). We have to keep in mind that we also see an average diffusion coefficient of macrolides (free and bound in micelles), according to equation 6. The lower the diffusion coefficient the more macrolides are bound to the micelles.

We can observe a rather high D of AGL and DES dissolved in bile salt, indicating lots of free macrolides are left in solution. In the case of ERI and AZA the diffusion goes down, because more macrolides are bound in the micelles. ADH and KLA show an extremely low diffusion coefficient very close to the absolute minimum. The mean value of KLA is even under the minimum, which is impossible, because there should not be bigger aggregates in solution than the micelles. But the error bars indicates that with considerations of the standard deviation the value can be over the minimum.

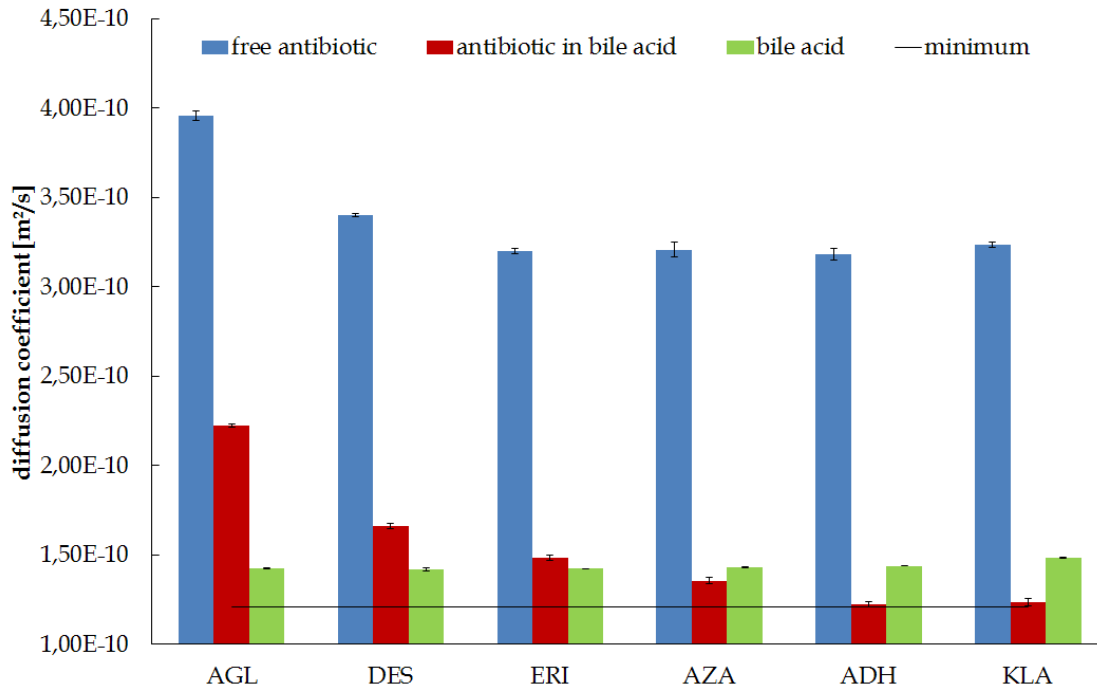


Figure 14: The overall results of the diffusion experiments with NaDCh. The values of free antibiotics are identical to figure 13. The minimum is calculated with equation 6 again.

The values of the NaDCh experiments (figure 14) show quite similar results to the NaCh. Again, the bile acid diffusions are similar over all macrolides suggesting no size influence and a good reproduceability. One difference compared to NaCh measurements is D of ERI and AZA, which was quite similar in NaCh. But the question remains, if this is really an effect of NaDCh or just method inaccuracy. The diffusion coefficients of ADH and KLA are again at the very bottom of the possible diffusion coefficient range.

If we compare the diffusion coefficients of NaCh at CMC and 100mM and NaDCh at CMC and 50mM with previous works in the literature (table 3), we got huge varying results. Especially [23] has similar results, but for the concentrations for D of micelles (D2, D4) are not declared in this paper. But in all cases the the values are in the same region, and more importantly they show the same pattern. The diffusion is always higher in the small concentration region (D1, D3) and NaCh (D1, D2) shows a lower diffusion coefficients than NaDCh (D3, D4).

Table 3: Diffusion Coefficients of NaCh at CMC (D1), at 100mM (D2) and NaDCh at CMC (D3) and 50mM (D4). All values for $D \cdot 10^{-10}$ [m²/s].

D1	D2	D3	D4	literature
3.79	1.44	3.96	1.21	our results
4.0	1.9	-	-	[24]
6.3	4.6	-	-	[25]
6.4 ± 0.1	5.0	7.0 ± 0.1	4.6	[26]
4.25	1.5 ± 0.1	4.83	1.3 ± 0.1	[23]

1.3.6 Mole fraction partition coefficient calculations

To get a value for the tendency of a macrolide going into the micelles, we used the mole fraction partition coefficient (K_p). K_p is defined by equation 7 and is the molar ratio of bound and free macrolide. When more macrolide is bound in the micelles, the mole fraction partition coefficient increases.

$$K_p = \frac{A_{\text{bound}}}{A_{\text{free}}} \quad (7)$$

Rewriting equation 6, considering $A_{\text{tot}} = A_{\text{bound}} + A_{\text{free}}$ and simplifying the compound fraction, the formula gives rise to the quite simple equation 8.

$$K_p = \frac{A_{\text{bound}}}{A_{\text{free}}} = \frac{D_{\text{exp}} - D_{\text{free}}}{D_{\text{bound}} - D_{\text{exp}}} \quad (8)$$

D_{exp} is the diffusion of the macrolide in the bile acid solution, D_{bound} the diffusion coefficient of the micelles (minimum) and D_{free} the diffusion of the free macrolide. Table 9 shows the results of this calculation for every macrolide in both bile acid micelles. Figure 15 visualizes this table for a better understanding.

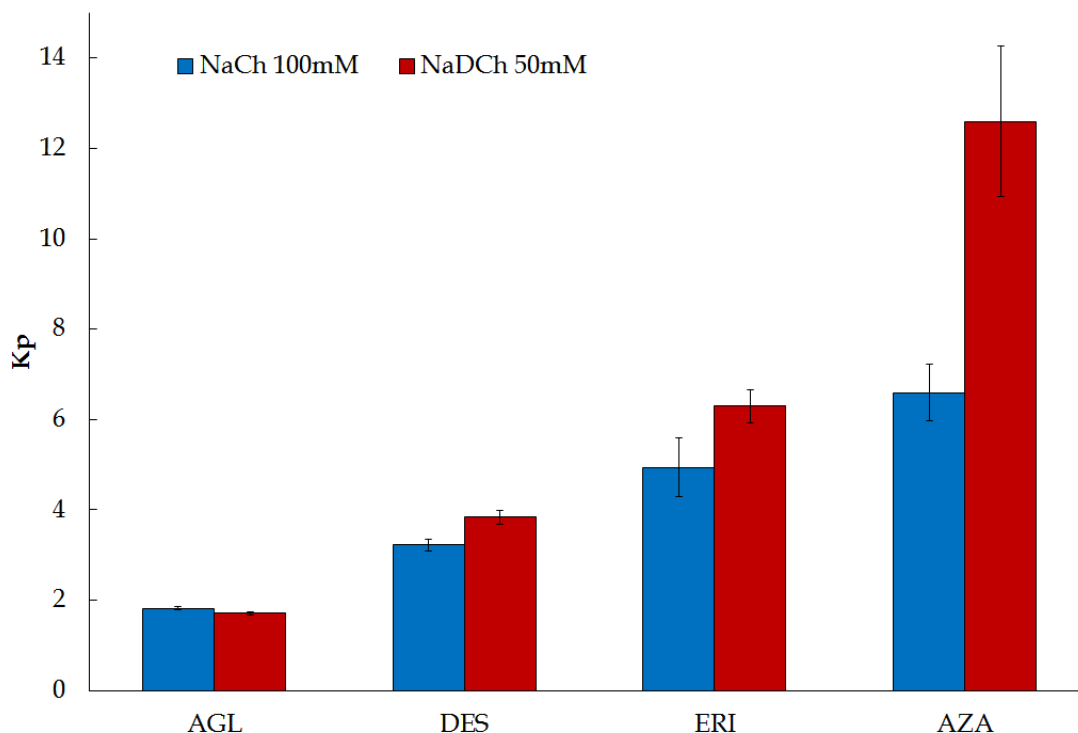


Figure 15: The mole fraction partition coefficient of all macrolides. ADH and KLA are not plotted, because their values are higher all than 40. The actual results for these two macrolides are visible in table 9 in the appendix.

In case of ADH and KLA the mean values of D_{exp} or at least their error bars goes under D_{bound} , which would end up in a meaningless negative mole fraction partition coefficient, according to equation 8. Therefore, by using the maximum possible value of D_{exp} (mean value + standard deviation), the lowest possible mole fraction partition coefficient is calculated. For this calculation we used the mean values for D_{bound} and D_{free} . However, this is not the most accurate prediction of K_p , but at least an indication for the actual value.

AGL shows the lowest K_p value (approx. 2), indicating the molar ratio of bound to free macrolide of 2:1. DES has also a rather high amount of free macrolides. When we get to ERI and AZA with their K_p values of about 6-10, we see that only 10-20 % of the macrolides remain in solution. Also the error bars are getting quite high because of the characteristics of error prolongation (eq. 2). As we could indicate from figure 13 and 14

nearly everything of ADH and KLA is bound in the micelles (table 9 in appendix). It is also visible that the macrolides bind rather to the NaDCh micelles than to the NaCh micelles.

All these effects can be explained by the same physical property as in the concentration measurement section: polarity and furthermore hydrophilicity. As discussed before, the polarity is going down like: $AGL > DES > ERI \approx AZA > ADH \approx KLA$. The micelles with their apolar core can dissolve hydrophobic macrolides better than the hydrophilic ones. This is also the reason why macrolides in the more apolar NaDCh shows higher mole fraction partition coefficients.

1.4 Conclusion

Although the fact that our approach has difficulties with the small concentrations of macrolides compared to the bile acid, our experiments showed that the method is a good and powerful tool for distribution investigations of free and bound species. One solution of this problem would be to use fully deuterated bile acids. This would vanish the interfering bile acid peaks, but unfortunately they are not commercially available. The overall conclusion of this investigations is that the main parameter for solubility and mole fraction partition coefficient is polarity. The more apolar a macrolide, the higher is the tendency to bind to micelles. Further investigations should be done on this topic. It would be important to investigate on this polarity dependence, by using bile acids with different polarities, for instance lithocholic acid (only one OH group left, apolar) or taurocholic acid (taurin amid derivative of cholic acid, polar). Also macrolide antibiotics with derivatised sugar units can be measured on this matter.

2 A general method for diagonal peak suppression in homonuclear correlated NMR spectra by spatially and frequency selective pulses

2.1 Introduction

In a typical 2D homonuclear correlated spectrum the diagonal contains the most intense peaks, although all the relevant information is contained in the cross peaks. These intense signals can obscure nearby cross peaks. Furthermore, the diagonal is often responsible for the so called t_1 -noise, artifacts along the indirect dimension. Intense diagonal peaks also limit the dynamic range of the spectrometer, leading to a lower sensitivity of low intensity signals. The stronger the diagonal peaks in relation to the cross peaks are, the bigger are the problems they cause. In particular, NOESY-type spectra, where the intensity ratio of diagonal versus cross peaks is quite extreme, often suffer from strong diagonal peak artifacts which can easily obscure nearby cross peaks.

Several different strategies for diagonal peak suppression have been reported in the literature. The first approach is based on suppressing diagonal peaks by recording two spectra, a regular 2D spectrum and one containing only the diagonal [27][28]. The latter is obtained by setting the mixing time to zero. Subtraction of the diagonal-only spectrum from the regular one provides a diagonal-free spectrum. However, this approach only works if there is no significant relaxation during the mixing time and does not alleviate the t_1 -noise or dynamic range problem since one still has to record datasets with a diagonal. In addition, by using this technique, the acquisition of two different comparable spectra requires a high accuracy of the parameter settings. Otherwise subtraction artifacts will lead to insufficient suppression of the diagonal [28][29][30].

The second method destroys the magnetization of the excited nucleus by a defocus, mixing, refocus sequence [31]. The mixing period is implemented between two 90° pulses. The magnetization of the excited nucleus, which has not been transferred during the mixing period, undergoes a 180° rotation. A last 90° pulse transfers this magnetization into the z-direction leading to no visible signal of the diagonal in the spectrum. This method leads to an unusual appearance of the 2D spectra, showing cross peaks on diagonals with a slope $\Delta\omega_1/\Delta\omega_2 = 2$.

Another method, which has been used to suppress diagonal peaks in a NOESY spectrum uses a combination of two jump-and-return sequences before and after the mixing and a pulsed field gradient to suppress magnetization that evolved with the same frequencies before and after mixing [32]. By this approach the signal intensities in the 2D spectrum are modulated by a sheared sinusoidal profile with zero intensity on the diagonal as a result of the jump-and-return sequences.

For multidimensional (3D and 4D) ^{15}N -edited NOESY-type spectra the suppression of diagonal peaks has also been described by selecting only magnetization transfer pathways where the spin-state has been changed. This approach, which allows the observation of cross peaks underneath the diagonal, only works on TROSY-type spectra on proteins and for ^{15}N -bound protons [33][34][35][36][37][38][39]. Especially for 3- and 4D NOESY type spectra diagonal peak suppression is very convenient, as it makes the use of sparse data sampling techniques much easier due to a significant reduction of the spectral dynamic range [10; 11].

2.2 Theory and method

Here we present a completely different, generally applicable, approach for diagonal peak suppression in homonuclear two- and multidimensional spectra, which is based on transforming a homonuclear system into a spatially-separated heteronuclear system by using frequency-selective pulses during a weak field gradient [40][41][42][43][44][45][46]. To obtain a diagonal peak suppressed homonuclear 2D spectrum we use the pulse sequences shown in figure 16. A selective 90° pulse during a weak gradient excites different signals in different slices of the NMR sample tube. After the mixing period (shown for TOCSY and NOESY type spectra) the excited signals that did not change their frequency significantly during mixing (i.e. the diagonal peak signals but also any underlying or very close-by cross peaks) can be suppressed by using any signal/solvent suppression scheme, when applied during the same weak gradient field. For this purpose we used an excitation sculpting scheme (a combination of a hard and a selective 180° pulse sandwiched by two strong gradients) [47]. To increase the efficiency of the diagonal suppression this element was repeated with different purging gradient strength.

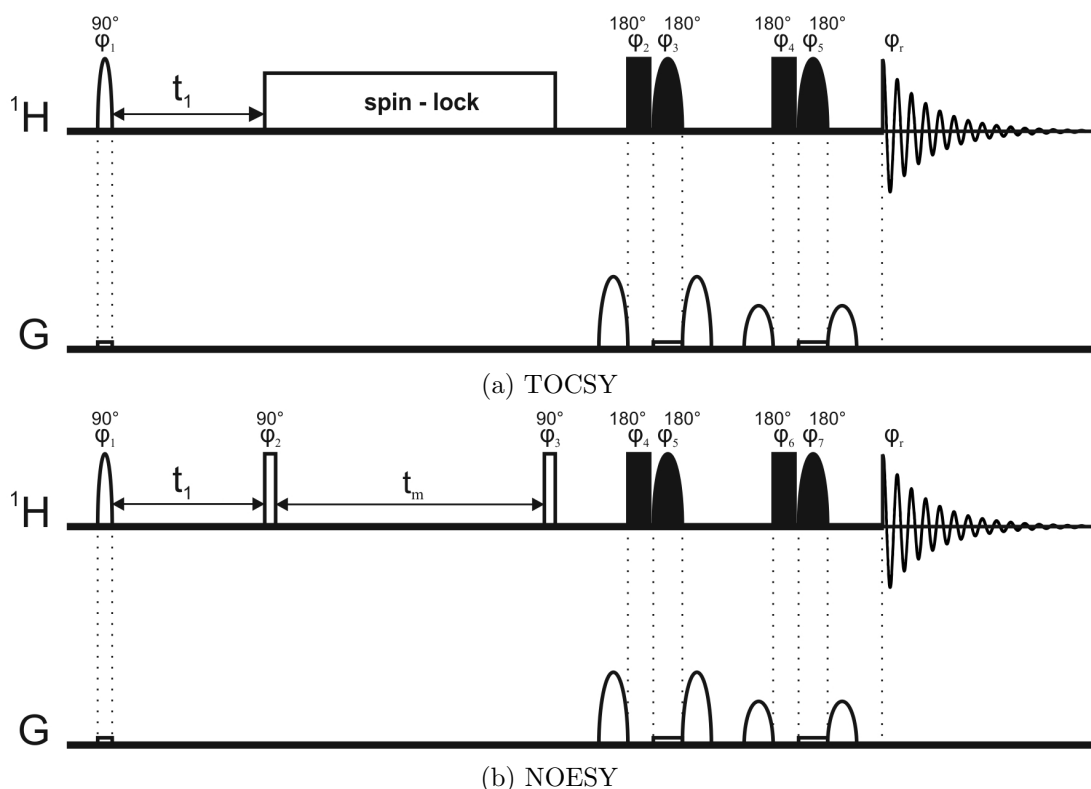


Figure 16: The pulse sequence of a diagonal suppressed TOCSY experiment is shown in a). The slice-selective excitation is achieved by a 40 ms EBURP-2 pulse, applied during a weak magnetic field gradient (approx. 1 Gauss/cm). After the evolution and TOCSY mixing, for which we used a 12.5 kHz DIPSI-2 sequence at 500 MHz, the originally excited magnetization, which would produce the diagonal peaks is suppressed by two consecutive excitation sculpting blocks. The latter contain 4 ms rectangular shaped selective 180° pulses during a field gradient which has the same strength of the one used during initial excitation. The following phase cycling was used for a: $\phi_1 = x, -x$; $\phi_2 = x, x, y, y$; $\phi_3 = -x, -x, -y, -y$; $\phi_4 = x, x, x, x, y, y, y, y$; $\phi_5 = -x, -x, -x, -x, -y, -y, -y, -y$; $\phi_r = x, -x, -x, x, -x, x, x, -x$. The pulse sequence of a diagonal suppressed NOESY experiment is shown in b). The selective 90° and 180° pulses are the same as in a). The phase cycle for b is: $\phi_1 = x, x, -x, -x$; $\phi_2 = x$; $\phi_3 = x, x, x, x, -x, -x, -x, -x, y, y, y, y, -y, -y, -y, -y$; $\phi_4 = \phi_6 = x, x, x, x, y, y, y, y$; $\phi_5 = -x, -x, -x, -x, -y, -y, -y, -y$; $\phi_7 = x, y$; $\phi_r = x, -x, -x, x, x, -x, -x, x, y, -y, -y, y, y, -y, -y, y$. 90° and 180° pulses are indicated by white and black bars, respectively.

The method of spatially dependent selective spin excitation in solution NMR has been used previously, for example for homonuclear broadband decoupling [40][41][42][43][44][46].

Because of the weak field gradient, the resonance frequencies of the NMR signals are shifted, depending on the position in the sample. The range of frequency shifts of these signals is given by equation 9

$$\Delta\omega = s \cdot G \cdot \gamma \quad (9)$$

where G is the strength of the gradient, γ is the gyromagnetic ratio and s is the sample length to be measured, in our case about 1cm. Therefore, if we want to use a selective pulse to excite a range of 10 ppm of a proton spectrum on a 500 MHz spectrometer we need at least a gradient strength of 1.2 G/cm. The spatial dependence of the resonance frequencies is shown in figure 17.

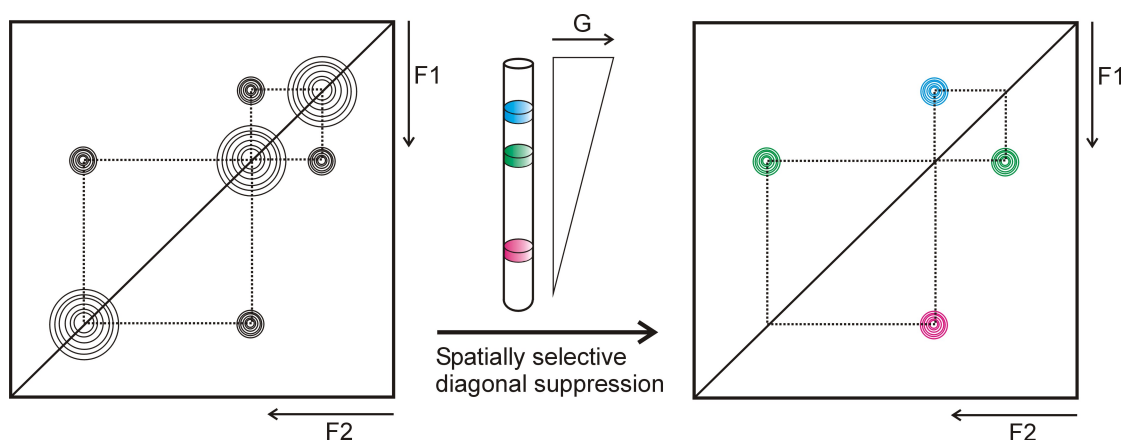


Figure 17: The principle of the selective excitation during a weak field gradient: Small, continuous, variations of the magnetic field lead to a shifting of the spectrum. A selective pulse applied in the middle leads to the excitation of all resonances, but each signal is irradiated in a different slice of the sample tube. A schematic example of a diagonal suppressed homonuclear 2D spectrum, where proton 2 (green) correlates with proton 1 (blue) and 3 (pink), but 1 not directly with 3. Auto-correlation (diagonal) peaks are suppressed by using an excitation sculpting block on the signals that were originally, selectively excited in the same slice.

For a better understanding we illustrate the presented method by a hypothetical molecule. The molecule has 3 protons with different chemical shifts and only the proton with the resonance frequency f_2 (green) shows a correlation to the other two protons 1 (blue) and 3 (pink) (fig. 17), whereas 1 is not directly correlated with 3. In the slice x_1 the selective pulse only excites the nuclei with frequency f_1 (blue), in x_2 only f_2 (green) and in x_3

only f_3 (pink). During t_1 the chemical shift in the indirect dimension evolves. If we stop the experiment here, Fourier transformation would yield a 2D spectrum where only the diagonal peaks are visible.

During the mixing period, the magnetizations of the individual nuclei are partly transferred to their correlation partners. The polarization of f_2 is partly moved to the nuclei with f_1 and f_3 . The magnetization at x_1 is transferred from protons with f_1 to protons with f_2 and at x_3 some magnetization is now at protons with f_2 . If we would end the experiment at this point, the appearance of the resulting spectrum would be like a regular 2D spectrum including diagonal- and cross peaks. Subsequently, the magnetization which is on-resonance during the weak gradient field is destroyed by two excitation sculpting blocks. So, the part of the magnetization that is not transferred during the mixing sequence, and which produces the diagonal peak is removed right before the start of acquisition.

The result is that in slice x_1 the only remaining magnetization is from protons with f_3 (top blue peak in fig. 17). In slice x_2 protons with f_2 in the indirect dimension have remaining magnetizations of f_1 and f_3 (green peaks) and in slice x_3 protons with f_3 in t_1 have peaks at f_2 (bottom pink peak). Correlation peaks which are underneath the diagonal (from two correlated nuclei which happen to have the same chemical shift) are of course also suppressed by this method and cannot be observed. This spatially-selective approach for diagonal peak suppression can be applied to any kind of homonuclear two- (and multi-) dimensional NMR spectrum simply by replacing the first 90° excitation pulse by a selective one applied during a weak gradient and using an on-resonance signal suppression scheme right before acquisition, which is also applied during a weak gradient field. Due to the slice-selective excitation the sensitivity of the proposed scheme is reduced when compared to a regular 2D experiment. It is determined by the width of the excitation slice. The width of this slice is determined by the strength of the gradient (approx. 1-1.5 G/cm to excite all protons in the spectrum). We used typically a gradient of 1.5G/cm, which covers approx. 10 ppm ^1H frequency at 500 MHz. The width of the excited sample slice is also determined by the width of the excitation pulse. On the other hand the selectivity of the pulse determines how close signals can be to the diagonal to still be observable. However, if the pulse gets too selective, the excited sample slices gets smaller, which reduces the sensitivity.

The thickness of the slice excited during the weak gradient corresponds to the ratio $\Delta\omega_{\text{ex}}/\Delta\omega$, with $\Delta\omega_{\text{ex}}$ being the excitation bandwidth of the selective pulse and $\Delta\omega$ the frequency shift range induced by the weak gradient in the detected sample volume length. Therefore, the reduction percentage in signal/noise $\Delta(S/N)$ of a spatially selectively excited spectrum compared to a regular one is given by equation 10.

$$\Delta \frac{S}{N} = \frac{\Delta\omega_{\text{ex}}}{\gamma \cdot G \cdot s} \quad (10)$$

For the selective pulse it is also important that it does not produce excitation sidebands and gives little phase distortions across the excitation region. We obtained best results using an E-BURP2 shaped pulse [48] for excitation. As a compromise between selectivity and sensitivity we employed a 40 ms pulse. The selective 180° pulse used in the excitation sculpting blocks is less demanding as far as the excitation profile is concerned and we typically used a 4 ms square pulse. The longer this “purging” pulse is the sharper the region around the diagonal which is suppressed.

However, this pulse cannot be made too selective due to diffusion between the excitation and the diagonal suppression. Diagonal peaks which are excited at the beginning in a very narrow slice then start to diffuse during the pulse sequence and it is important that the pulse used during the excitation sculpting block acts on all spins that were excited in a slice, including the ones that changed their location by diffusion. Therefore, the width of the suppressed diagonal can be made narrower for larger, more slowly diffusing molecules. In the case of negligible diffusion during the pulse-sequence (proteins and other large molecules) the bandwidth of the selective pulse used to suppress the diagonal peaks can be as narrow as the original excitation pulse. However, the purging pulse must not be more selective than the excitation pulse since this would lead to cancellation of diagonal peaks in slices narrower than the excitation slices and therefore reintroduce diagonal peaks from nearby sample tube regions.

One nice feature, inherent to slice-selective excitation, is its insensitivity to poor shimming (magnetic field inhomogeneities) along the z-direction [49]. Therefore, the signals obtained in our diagonal-suppressed spectra are characterized by very narrow line-widths, even if the magnetic field is not very homogenous.

NOESY spectra of lysozyme were recorded on a Bruker AVANCE III 700 MHz NMR spectrometer using a 5 mm TCI cryo probe at 298 K. All other spectra were acquired on a Bruker AVANCE III 500 MHz spectrometer using a 5 mm TCI probe at 298K. For all 2D experiments data matrices of 1024 x 128 complex data points were acquired and, after zero filling to twice the number of points, multiplied by a 60° phase-shifted squared sine-bell window function in both dimensions. The highly derivatized sugar methyl-4,6-O-benzylidene-2,3-O-ditosyl- α -glucopyranoside was obtained from Prof. Karl Dax at the Graz University of Technology. All other compounds were from Sigma Aldrich (St. Louis, USA) in the highest purity available.

2.3 Results and discussion

As test examples for the presented approach we acquired diagonal peak free TOCSY and NOESY spectra of a highly substituted monosaccharide (methyl-4,6-O-benzylidene-2,3-O-ditosyl- α -glucopyranoside [50]) dissolved in CDCl₃ as well as a diagonal-free NOESY spectrum of the protein lysozyme (14 kDa). In solution, methyl-4,6-O-benzylidene-2,3-O-ditosyl- α -glucopyranoside partly loses its benzylidene moiety and consists of an almost equimolar mixture of the fully protected and 4,6-deprotected form (figure 18).

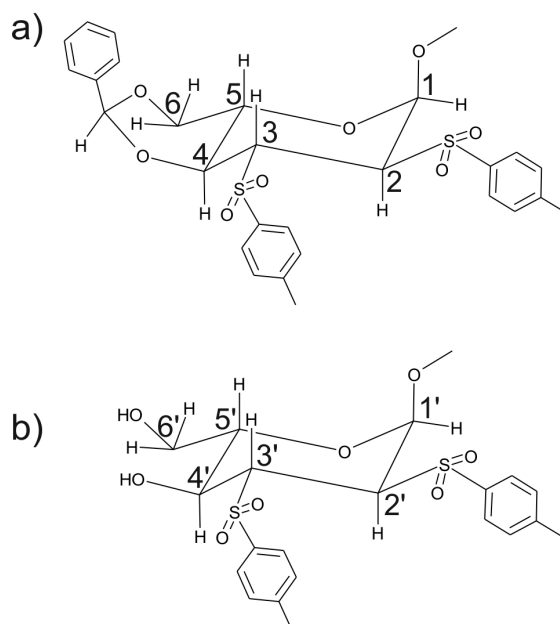


Figure 18: The chemical structures of a) methyl-4,6-O-benzylidene-2,3-O-ditosyl- α -glucopyranoside and its degradation product b) methyl-2,3-O-ditosyl- α -glucopyranoside.

The regular TOCSY of methyl-4,6-O-benzylidene-2,3-O-ditosyl- α -glucopyranoside (60mg dissolved in 600 μ l CDCl₃) (fig. 20a in appendix) was recorded with 8 scans and 16 were accumulated for the diagonal peak suppressed version (fig. 20b in appendix).

Both spectra were recorded with a mixing time of 80 ms and 6000 Hz spectral width in both dimensions. All diagonal peaks are completely removed in the diagonal suppressed version while peaks close to it can still be observed. The width of the diagonal suppressed region depends on the selectivity of the pulse used for the excitation sculpting. In our case a 4ms square pulse was employed but it should be changed to a longer, more selective pulse if signals even closer to the diagonal need to be observed. The lower sensitivity of the diagonal-free spectrum, which results from the slice selective excitation during the gradient can be somewhat compensated by increasing the receiver gain because of the absence of strong diagonal peaks. For molecules which require smaller spectral widths the strength of the weak gradient can be reduced which increases the signal/noise ratio. The higher resolution of the diagonal-free spectrum results from the better magnetic field homogeneity in the slices where the signals are detected [32] compared to the complete detected sample volume of a regular TOCSY.

Artifacts from the diagonal are typically much more severe in NOESY type spectra. Especially the weak NOEs of small molecules ($\omega\tau_c < 1$) often lead to cross peaks which are hidden in the tails of huge nearby diagonal peaks. This can be seen in figure 21 in the appendix, which shows a close up of a regular (top) and diagonal peak suppressed 2D NOESY (bottom) of methyl-4,6-O-benzylidene-2,3-O-ditosyl- α -glucopyranoside with mixing times of 700 ms.

Positive and negative peaks are colored red and blue, respectively. Close to the diagonal it is difficult to differentiate artifacts from real peaks in the regular NOESY spectrum. This is most pronounced in the region between 3.1 – 3.8 ppm. Some peaks are visible only in the diagonal-free spectrum (indicated by arrows), while others are stronger in the regular NOESY (marked by asterisks). All peaks which are stronger in the regular NOESY correspond to signals that show strong diagonal peaks. On the other hand the peaks which are seen only in the diagonal free spectrum have relatively weak diagonal peaks in the regular NOESY spectrum. This is probably a result of the elevated baseline along the ω_1 -direction. Cross peaks at the same ω_2 -frequency of a strong diagonal peak

appear stronger than they are. In the regular NOESY some of the very strong cross peaks have much weaker counterparts on their symmetrized position.

In contrast, the diagonal suppressed NOESY shows cross peak intensities which are much more similar on both sides of the diagonal. To confirm that all peaks observed in the diagonal-free NOESY are actual NOE peaks and not artifacts, their assignment is indicated. They all correspond to proton pairs which are close in space, like axial protons on the same side of the glucose ring (2-4 and 3-5) or neighboring protons (1-2, 1'-2'). The regular NOESY experiment (fig. 21a) was recorded with 32 scans per increment and the diagonal suppressed NOESY spectrum (fig. 21b) by using 256 scans per increment and otherwise identical parameters. To experimentally determine the signal/noise changes of the regular versus the spatially-selective, diagonal-suppressed NOESY spectrum, representative traces at the frequency 4.3 ppm for two short NOESY spectra recorded with the same acquisition parameters (number of scans, increments, receiver gain etc) and processing scheme is shown in figure 19. As expected, for a selective pulse with an excitation bandwidth of ~ 80 Hz and a 1.2 G/cm gradient the signal/noise ratio drops to about 2% of a regular NOESY spectrum.

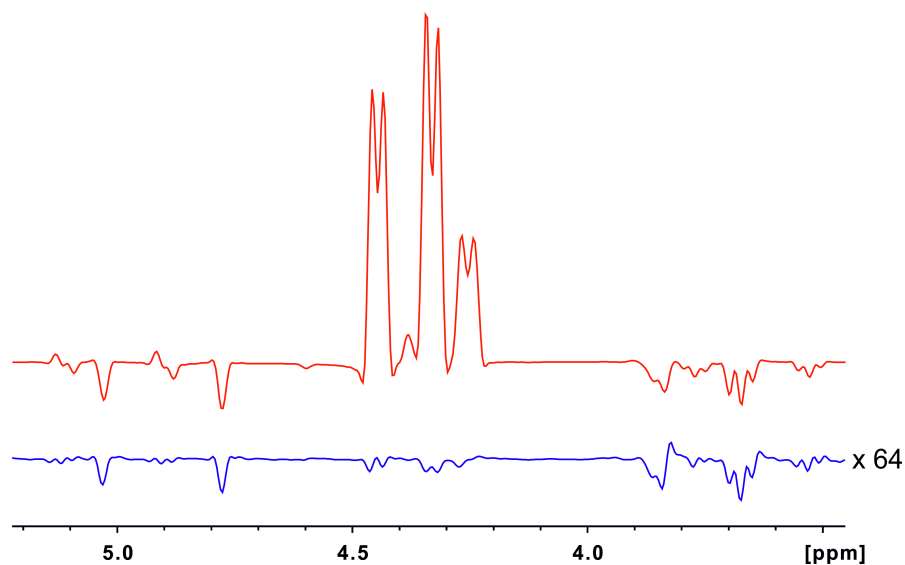


Figure 19: Traces taken along the signals at ~ 4.3 ppm in the indirect dimension of a short regular NOESY (red) and a diagonal suppressed version (blue) of the glucopyranosides with absolutely equal acquisition and processing parameters. The trace from the diagonal suppressed NOESY is multiplied by 64, showing the expected lower sensitivity of the slice-selective pulse sequence. For these comparative NOESY spectra 64 scans and 64 complex data points in the indirect dimension were recorded.

To evaluate the performance of the diagonal suppression scheme also on bigger, faster relaxing molecules, we acquired a diagonal suppressed NOESY spectrum of the 14 kDa protein lysozyme (3 mM) in D_2O solution. As can be seen in figure 22, the presented approach leads to a complete removal of all diagonal peaks, while the cross peaks are unaffected.

Both spectra were recorded with a mixing time of 150 ms and 8000 Hz spectral width in both dimensions. Sixty-four scans were acquired for the regular NOESY and 512 for the diagonal free version. The total duration of the pulse-sequence of the presented approach is not much longer than a regular NOESY. Only the first pulse is now 40 ms instead of the hard pulse and the diagonal suppression is technically the same as the typical solvent suppression. Therefore, any additional relaxation losses of the diagonal-free spectrum, relative to the regular experiment, are minimal. When solvent suppression is needed in diagonal-free spectra, we use presaturation of the water signal before the first selective

90° pulse, rather than adding another excitation sculpting / watergate sequence prior to acquisition to keep relaxation losses to a minimum.

2.4 Conclusions

We have presented a generally applicable approach to obtain diagonal peak free homonuclear correlated spectra. It relies on the slice selective excitation during a weak gradient field. Signals that do not change the frequency during the mixing are removed by excitation sculpting right before the acquisition. Due to this spatially selective excitation the magnetic field is very uniform for each signal and therefore cancels most of the magnetic field inhomogeneities along the z-direction. However, as a result, the sensitivity is reduced compared to a regular spectrum. To the best of your knowledge this is the first generally applicable diagonal peak suppression method which does not change the relative cross peak intensities or the appearance of the spectrum and does not rely on the subtraction of individual spectra.

References

- (1) Gaynor, M.; S., M. A. *Front. Med. Chem.* **2005**, *2*, 21–35 (cit. on p. 1).
- (2) Montenez, J.; Van Bambeke, F.; Piret, J.; R., B.; Tulkens, P.; Mingeot-Leclercq, M. *Toxicol. Appl. Pharmacol.* **1999**, *156*, 129–140 (cit. on p. 1).
- (3) Reasor, M. J.; Kacew, S. *Exp. Biol. Med.* **2001**, *226*, 825–830 (cit. on p. 1).
- (4) Kostrubsky, V. E.; Strom, S. C.; Hanson, J.; Urda, E.; Rose, K.; Burliegh, J.; Zocharski, P.; Cai, H.; Sinclair, J. F.; Sahi, J. *Toxicol. Sci.* **2003**, *76*, 220–228 (cit. on p. 1).
- (5) Kosol, S.; Schrank, E.; Krajacic, M. B.; Wagner, G. E.; Meyer, N. H.; Gobl, C.; Rechberger, G. N.; Zangger, K.; Novak, P. *J. med. Chem.* **2012**, *55*, 5632–5636 (cit. on p. 2).
- (6) Wiedmann, T. S.; Kamel, L. *J. Phar. Sci.* **2002**, *91*, 1743–1764 (cit. on p. 3).
- (7) Nawroth, T.; Buch, P.; Buch, K.; Langguth, P.; Schweins, R. *Mol. Pharmaceutics* **2011**, *8*, 2162–2172 (cit. on p. 3).
- (8) Hjelm, R.; Thiyagarajan, P.; Alkan-Onyuksel, H. *J. Phys. Chem.* **1992**, *96*, 8653–8661 (cit. on p. 3).
- (9) Leng, J.; Egelhaaf, S.; Cates, M. *Biophys. J.* **2003**, *85*, 1624–1646 (cit. on p. 3).
- (10) Mukhopadhyay, S.; Maitra, U. *Current Science* **2004**, *87*, 1666–1682 (cit. on p. 3).
- (11) Paesen, J.; Khan, K.; Roets, E.; Hoogmartens, J. *Int. J. Pharm.* **1994**, *113*, 215–222 (cit. on p. 4).
- (12) Zakrzewska, J.; markovic, V.; Vucelic, D.; Feigin, L.; Dembo, A.; Mogilevsky, L. *J. Phys. Chem.* **1990**, *94*, 5078–5081 (cit. on p. 4).
- (13) Lasch, J. *Biochim. Biophys. Acta* **1995**, *1241*, 269–292 (cit. on p. 4).
- (14) Claridge, T. D. W., *High-Resolution NMR Techniques in Organic Chemistry*; 2, 2008; Vol. 27, pp 303–334 (cit. on pp. 5, 12).

- (15) Ekwall, P.; Rosendahl, T.; Löfman, N. *Acta Chem. Scand. II* **1957**, *11*, 590–598 (cit. on p. 16).
- (16) De Venditis, E.; Palumbo, G.; Parlato, G.; Bocchini, V. *Anal. Biochem.* **1981**, *115*, 278–286 (cit. on p. 16).
- (17) Sugihara, G.; Yamakawa, K.; Murata, Y.; Tanaka, M. *J. Phys. Chem.* **1982**, *86*, 2784–2788 (cit. on p. 16).
- (18) Coello, A.; Meijede, F.; Rodriguez Nunez, E.; Vazquez Tato, J. *J. Pharm. Sci.* **1996**, *85*, 9–15 (cit. on p. 16).
- (19) Navas Diaz, A.; Garcia Sanchez, F.; Garcia Pareja, A. *Colloid Surface A* **1998**, *142*, 27–34 (cit. on p. 16).
- (20) Garidel, P.; Hildebrand, A.; Neubert, R.; Blume, A. *Langmuir* **2000**, *16*, 5267–5275 (cit. on p. 16).
- (21) Nakashima, T.; Anno, T.; Kanda, H.; Sato, Y.; Kuroi, T.; Jujii, H.; Nagadome, S.; Sugihara, G. *Colloid Surface B* **2002**, *24*, 103–110 (cit. on p. 16).
- (22) Posa, M.; Tepavcevic, V. *Colloid Surface B* **2011**, *86*, 285–291 (cit. on p. 16).
- (23) Mangiapia, G.; Paduano, L.; Ortona, O.; Sartorio, R.; D’Errico, G. *J. Phys. Chem. B* **2013**, *117*, 741–749 (cit. on pp. 16, 20).
- (24) Lindman, B.; Kamenka, N.; Brun, B. *J. Colloid Interface Sci.* **1976**, *56*, 328–336 (cit. on p. 20).
- (25) Hao, L.; Lu, R.; Leaist, D.; Poulin, P. *J. Solution Chem.* **1997**, *26*, 113–125 (cit. on p. 20).
- (26) Mangiapia, G.; D’Errico, G.; Capuano, F.; Ortona, O.; Heenan, R. K.; Paduano, L.; Sartorio, R. *Phys. Chem. Chem. Phys.* **2011**, *13*, 15906–15917 (cit. on p. 20).
- (27) Bodenhausen, G.; Ernst, R. R. *Mol. Phys.* **1982**, *47*, 319–328 (cit. on p. 23).
- (28) Denk, W.; Wagner, G.; Rance, M.; Wüthrich, K. *J. Magn. Reson.* **1985**, *62*, 350–355 (cit. on p. 23).

- (29) Dalvit, C.; Bovermann, G.; Widmer, H. *J. Magn. Reson.* **1990**, *88*, 432–439 (cit. on p. 23).
- (30) Nagayama, K.; Kobayashi, Y.; Kyogoku, Y. *J. Magn. Reson.* **1983**, *51*, 84–94 (cit. on p. 23).
- (31) Harbison, G. S.; Feigon, J.; Ruben, D.; Herzfeld, J.; Griffin, R. G. *J. Am. Chem. Soc.* **1985**, *107*, 5567–5569 (cit. on p. 23).
- (32) Baur, M.; Kessler, H. *Magn. Reson. Chem.* **1997**, *35*, 877–882 (cit. on pp. 24, 30).
- (33) Diercks, T.; Truffault, V.; Coles, M.; Millet, O. *J. Am. Chem. Soc.* **2010**, *132*, 2138–2139 (cit. on p. 24).
- (34) Meissner, A.; Sørensen, O. W. *J. Biomol. NMR* **2001**, *19*, 69–73 (cit. on p. 24).
- (35) Pervushin, K. V.; Wider G. Riek, R.; Wüthrich, K. *P. Natl. Acad. Sci. USA* **1999**, *96*, 9607–9612 (cit. on p. 24).
- (36) Wen, J.; Zhou, P.; Wu, J. *J. Magn. Reson.* **2012**, *218*, 128–132 (cit. on p. 24).
- (37) Werner-Allen, J. W.; Coggins, B. E.; Zhou, P. *J. Magn. Reson.* **2010**, *204*, 173–178 (cit. on p. 24).
- (38) Wu, J.; Fan, J. S.; Pascal, S. M.; Yang, D. *J. Am. Chem. Soc.* **2004**, *216*, 15018–15019 (cit. on p. 24).
- (39) Zhu, G.; Xia, Y.; Sze, K. H.; Yan, X. *J. Biomol. NMR* **1999**, *14*, 377–381 (cit. on p. 24).
- (40) Aguilar, J. A.; Colbourne, A. A.; Cassani, J.; Nilsson, M.; Morris, G. A. *Angew. Chem. Int. Ed. Engl.* **2012**, *51*, 6460–6463 (cit. on pp. 24 sq.).
- (41) Aguilar, J. A.; Faulkner, S.; Nilsson, M.; Morris, G. A. *Angew. Chem. Int. Ed. Engl.* **2010**, *49*, 3901–3903 (cit. on pp. 24 sq.).
- (42) Aguilar, J. A.; Nilsson, M.; Morris, G. A. *Angew. Chem. Int. Ed. Engl.* **2011**, *50*, 9716–9717 (cit. on pp. 24 sq.).

- (43) Meyer, N. H.; Zangger, K. *Angew. Chem. Int. Ed. Engl.* **2013**, revised version submitted (cit. on pp. 24 sq.).
- (44) Nilsson, M.; Morris, G. A. *Chem. Commun.* **2007**, 933–935 (cit. on pp. 24 sq.).
- (45) Wagner, G. E.; Sakhaei, P.; Bermel, W.; Zangger, K. *Chem. Commun.* **2013**, 3155–3157 (cit. on p. 24).
- (46) Zangger, K.; Sterk, H. *J. Magn. Reson.* **1997**, *124*, 486–489 (cit. on pp. 24 sq.).
- (47) Hwang, T. L.; Shaka, A. J. *J. Magn. Reson.* **1995**, *112*, 275–279 (cit. on p. 24).
- (48) Geen, H.; Freeman, R. *J. Magn. Reson.* **1991**, *93*, 93–141 (cit. on p. 28).
- (49) Bax, A.; Freeman, R. *J. Magn. Reson.* **1980**, *37*, 177–181 (cit. on p. 28).
- (50) Ohle, H.; Spencker, K. *Ber. Dtsch. Chem. Ges.* **1928**, *61*, 2387–2392 (cit. on p. 29).

Appendix

Table 4: Relevant data of the concentration experiments.

	antibiotic	bile acid	c(antibiotic) [mM]
AGL	0.99 ± 0.00	19.46 ± 0.20	5.10 ± 0.06
DES	0.98 ± 0.01	33.93 ± 0.34	2.89 ± 0.05
ERI	1.11 ± 0.12	67.13 ± 0.84	1.65 ± 0.18
AZA	1.01 ± 0.10	141.16 ± 1.58	0.72 ± 0.07
ADH	0.98 ± 0.07	137.82 ± 1.27	0.71 ± 0.05
KLA	0.92 ± 0.09	149.81 ± 2.22	0.62 ± 0.06

Table 5: Relevant data of the concentration experiments.

	antibiotic	bile acid	c(antibiotic) [mM]
AGL	1.00 ± 0.02	8.93 ± 0.12	5.57 ± 0.14
DES	0.98 ± 0.04	13.77 ± 0.26	3.54 ± 0.16
ERI	1.11 ± 0.12	33.75 ± 0.33	1.64 ± 0.17
AZA	0.99 ± 0.07	43.25 ± 0.32	1.14 ± 0.08
ADH	0.95 ± 0.04	68.59 ± 0.99	0.70 ± 0.03
KLA	1.00 ± 0.03	78.90 ± 0.63	0.63 ± 0.02

Table 6: CMC investigation of NaCh. Diffusion coefficient values for $D \cdot 10^{-10}$ [m²/s].

concentration	8	10	11	12	13	14	15	17	20
mean value	3.80	3.78	3.79	3.76	3.64	3.59	3.57	3.47	3.25
standard deviation	0.01	0.03	0.03	0.01	0.03	0.01	0.01	0.01	0.02

Table 7: CMC investigation of NaDCh. Diffusion coefficient values for $D \cdot 10^{-10}$ [m²/s].

concentration	2	3	4	5	6	8	10	12
mean value	4.01	3.93	3.94	3.84	3.70	3.40	3.13	2.85
standard deviation	0.03	0.03	0.03	0.02	0.02	0.01	0.01	0.02

Table 8: Diffusion coefficients of all samples. All values for $D \cdot 10^{-10}$ [m^2/s].

	AGL	DES	ERI	AZA	ADH	KLA
free macrolide	3.955 ± 0.027	3.399 ± 0.009	3.199 ± 0.014	3.207 ± 0.042	3.181 ± 0.033	3.235 ± 0.014
NaCh	1.692 ± 0.002	1.697 ± 0.004	1.706 ± 0.007	1.710 ± 0.004	1.693 ± 0.001	1.676 ± 0.001
macrolide in NaCh	2.326 ± 0.010	1.896 ± 0.017	1.728 ± 0.037	1.664 ± 0.021	1.444 ± 0.036	1.407 ± 0.062
NaDCh	1.427 ± 0.003	1.420 ± 0.009	1.423 ± 0.001	1.433 ± 0.003	1.439 ± 0.000	1.485 ± 0.004
macrolide in NaDCh	2.223 ± 0.010	1.663 ± 0.016	1.483 ± 0.016	1.357 ± 0.019	1.223 ± 0.015	1.237 ± 0.021

Table 9: Mole fraction partition coefficient K_p of all samples.

	AGL	DES	ERI	AZA	ADH	KLA
NaCh	1.82 ± 0.038	3.22 ± 0.12	4.94 ± 0.64	6.60 ± 0.63	> 42.5	> 60.9
NaDCh	1.71 ± 0.033	3.83 ± 0.16	6.29 ± 0.38	12.60 ± 1.66	> 68.2	> 41.2

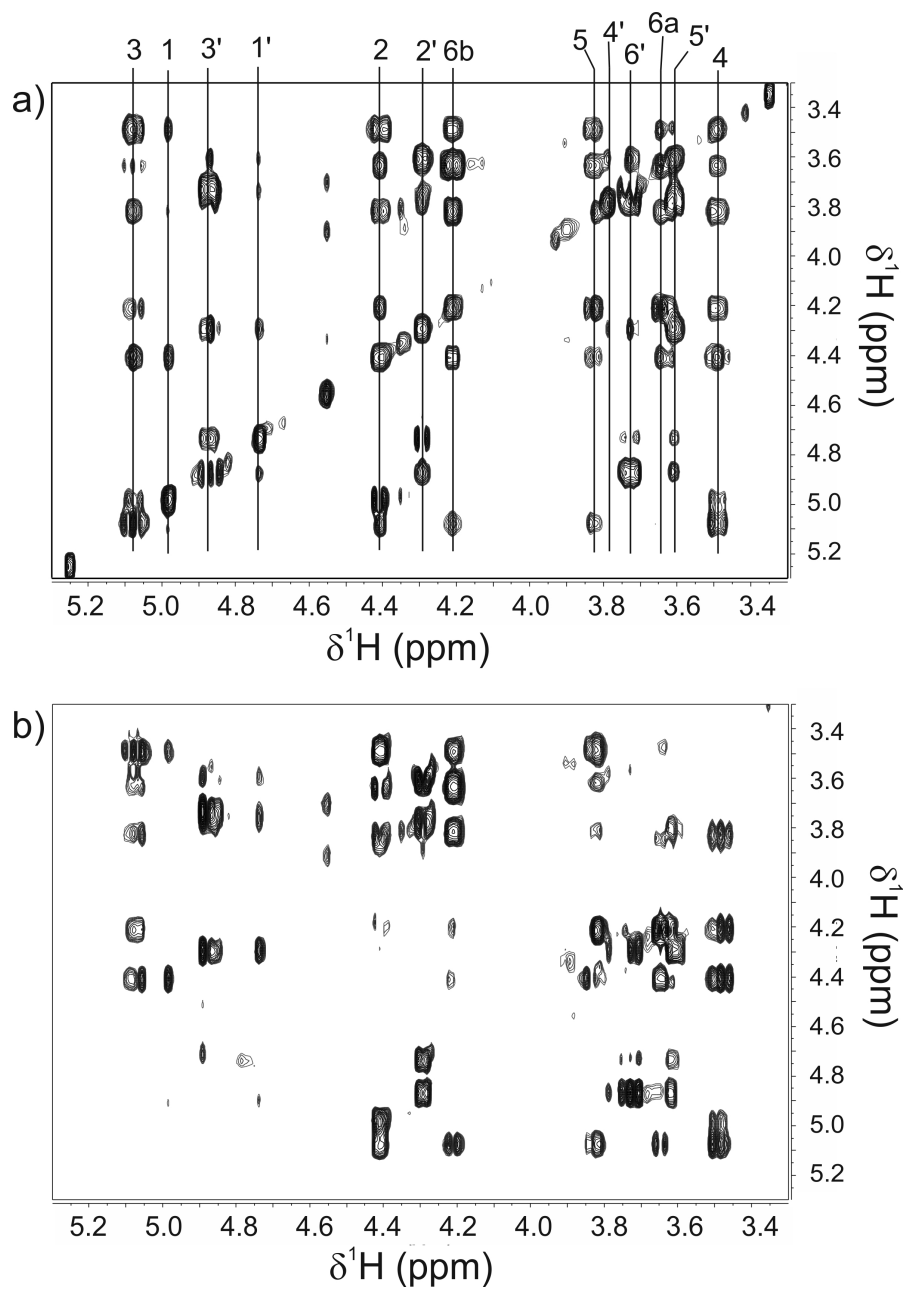


Figure 20: Close-up views of the most crowded regions of a regular TOCSY a) and diagonal suppressed version b) of the derivatized glucopyranosides. The increased resolution of the diagonal-free spectrum, which results from it being less affected by magnetic field inhomogeneities can be seen for example by better resolved scalar couplings of the signal at 3.5 ppm. The assignment (see figure 18 for the labeling scheme) is indicated in the regular TOCSY spectrum.

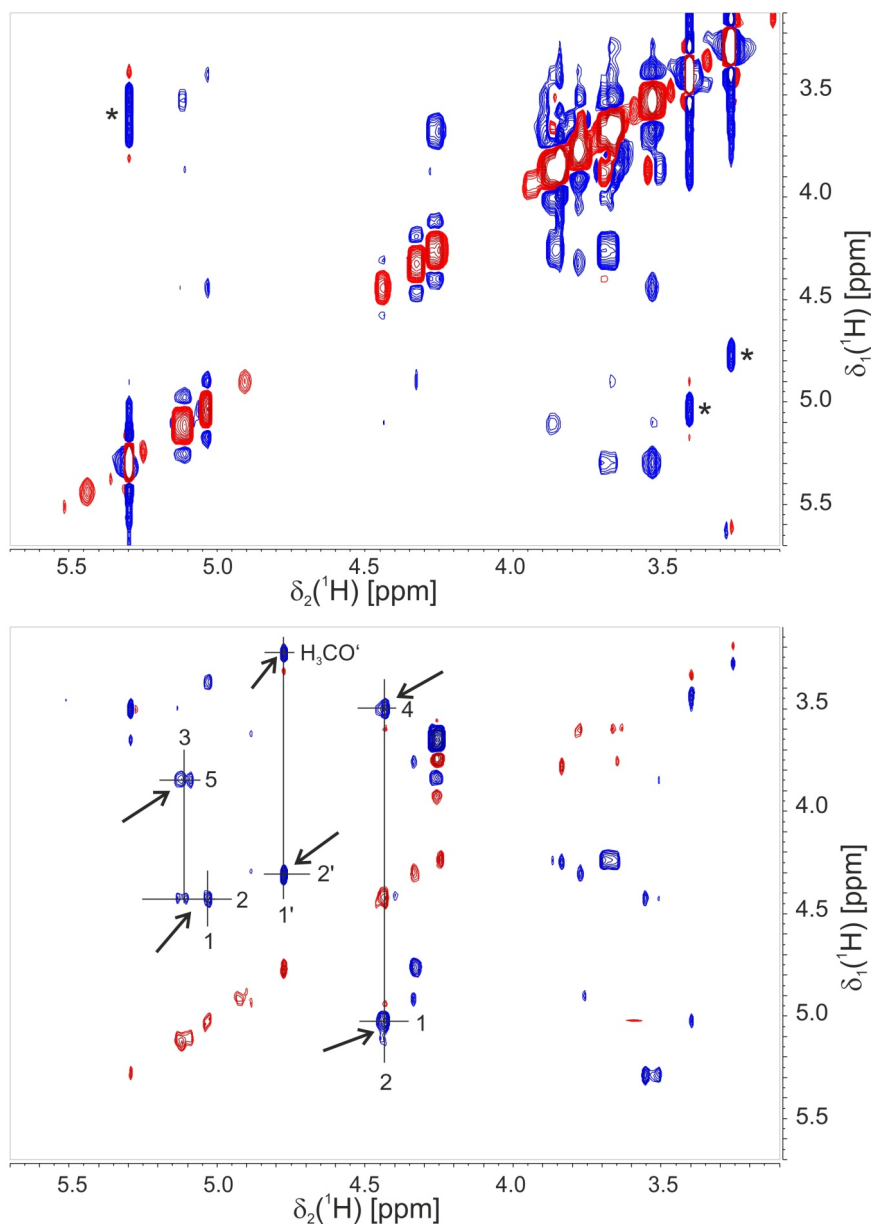


Figure 21: A close-up view of the most crowded region of a regular NOESY (top) and a diagonal-suppressed NOESY (bottom) spectrum of methyl-4,6-O-benzyliden-2,3-O-ditosyl- α -glucopyranoside. Positive and negative peaks are colored red and blue, respectively. Peaks that are made stronger by intense diagonal peaks are marked by asterisks. Signals which are more intense in the diagonal-free spectrum are assigned and indicated by arrows.

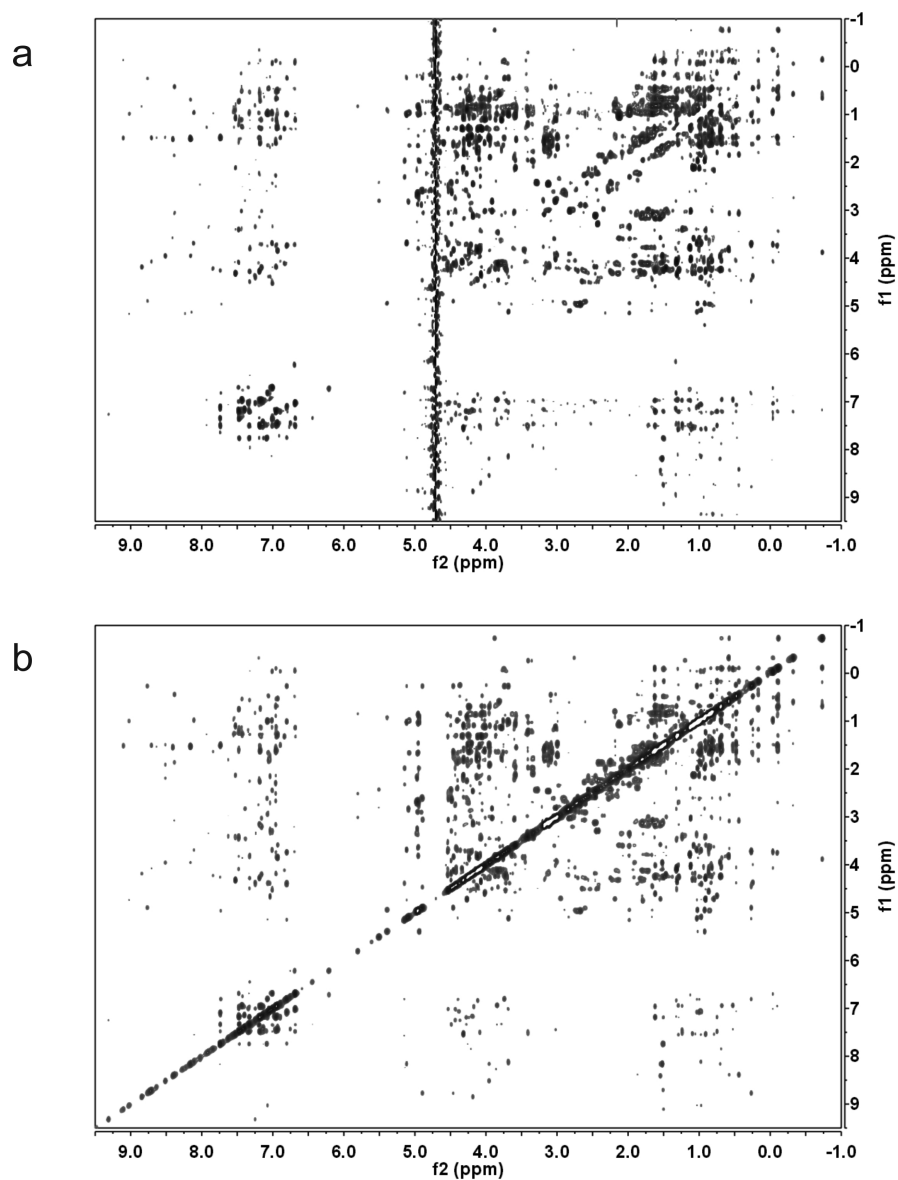


Figure 22: Diagonal-free a) and regular NOESY b) spectra of a 3 mM solution of lysozyme in D_2O . For both spectra 256 increments, with a spectral width of 8000 Hz were recorded. For the regular NOESY 64 scans were accumulated for each increment and 256 scans were used for the diagonal suppressed version. The mixing time was 150 ms.